In: Uranium: Compounds, Isotopes and Applications
Editor: Gerhardt H. Wolfe

ISBN 978-1-60692-573-7

Chapter 9

URANIUM MINERALS FROM A PORTUGUESE VARISCAN PERALUMINOUS GRANITE, ITS ALTERATION, AND RELATED URANIUM-QUARTZ VEINS

Marina M. S. Cabral Pinto[1,2,3], Maria M. V. G. Silva[1], Ana M. R. Neiva[1], Fernanda M. Guimarães[4] and Paulo B. Silva[4]

[1]Geosciences Center, Earth Sciences Department, University of Coimbra, Portugal, 3000-272 Coimbra, Portugal,

[2]Geosciences Department, University of Aveiro, Portugal, 3810 Aveiro Portugal

[3]University Jean Piaget of Cape Verde – Piaget Institute, Cidade da Praia, Caixa Postal 775, Santiago Island, Cape Verde

[4]LNEG–National Laboratory of Energy and Geology, Rua da Amieira, Apartado 1089, 4466-956 S. Mamede de Infesta, Portugal

ABSTRACT

A systematic study using scanning electron microscopy, X-ray maps and electron microprobe analyses was carried out on uranium minerals, such as uraninite, coffinite, saleeite, meta-saleeite, thorite and U-bearing minerals (xenotime, monazite, apatite, zircon) from unaltered and altered Variscan peraluminous granites and related hydrothermal brecciated uranium-quartz veins in order to study the release, migration, sorption and (re)precipitation of U during alteration under oxidizing conditions. Uraninite is magmatic and occurs mainly in the unaltered granite, is rare in the altered granite and was not found in the mineralized quartz veins. Uraninite from the altered granite is fractured and hydrated, has the radioactive damage halos filled with late pyrite, U-S-bearing phases and Fe oxyhydroxides and its analytical totals are lower than in the uraninite from the unaltered granite. The alteration zones and crystal rims are poorer in U (86.7 wt.% UO_2) than the cores and unaltered zones (90.2 wt.% UO_2) and some uraninite

[1] e-mail: marinacp@ci.uc.pt.

crystals are replaced by coffinite, which results from uraninite alteration. The U contents in coffinite crystals range between 65.0 wt.% UO_2 in the rims to 84.0 wt.% UO_2 in the cores of crystals. Thorite was found in all the granite samples and its composition is variable from 0.5 to 10.4 wt.% UO_2. Some thorite seems to be primary, whereas the other is related to the granite alteration and replaces apatite and monazite, is associated with xenotime, and fills fractures of several minerals. In the altered granite, thorite has low UO_2 contents (0.46 wt.%) in fractured crystal zones. Monazite from the altered granite has a pervasive porosity and some crystals were formed by alteration of apatite, and are frequently replaced by thorite. Monazite and xenotime from altered granite and hydrothermal veins have lower U contents than these minerals from unaltered granite. In the altered granite, xenotime crystals are zoned, with cores richer in U than the rims. Apatite from the altered granite is fractured, shows dissolution and has lower U and P contents than apatite from unaltered granite. In quartz veins, apatite crystals are replaced by uranium phosphates and have high U contents (~1.1 wt.% UO_2). In quartz veins, zircon rims have an extraordinary U enrichment (up to 18 wt.% UO_2). The most altered rims of chlorite and anatase from quartz veins are partially replaced by U-bearing Fe oxyhydroxides, containing up to 5.7 wt.% UO_2. Meteoric water warmed by deep circulation through granite faults, shear zones and quartz veins became enriched in U, P and Mg due to the solubilisation of mainly uraninite, coffinite, thorite and monazite, apatite, chlorite. Uranium from these solutions was later adsorbed on Fe oxyhydroxides, weathered surfaces of anatase, zircon and apatite, or precipitated as saleeite and meta-saleeite at the surface of Fe minerals and at apatite weathered surface due to local saturation.

Introduction

Uranium is a structural constituent in nearly two hundred mineral species (Fleischer and Mandarino 1995) and more than two hundred valid uranium-bearing mineral phases were compilated by Smith (1984). They are interesting as an energy resource and play a role in environmental problems associated with the disposal of radioactive waste materials, mining contamination and the remediation of contaminated sites. Therefore, the uranium minerals have been the subjects of an increase amount of attention (Burns and Finch 1999).

Uraninite is the most important uranium mineral in terms of abundance and economic value (Finch and Murakami 1999) and the principal ore mineral in the Portuguese uranium mineral deposits (Cotelo Neiva 2003). In general, it occurs in granites, pegmatites and associated quartz veins. Uraninite is unstable in acid and oxidizing conditions like those found in acid hydrothermal and meteoric fluids; it is easily dissolved and probably the most important source of dissolved U in groundwater emanating from weathered granite terrains (Basham et al. 1982, Poty et al. 1986, Cuney and Friedrich 1987, Tischendorf and Förster 1994, Plant et al. 1999, Förster 1999, Hecht and Cuney 2000). Other minerals from rocks (e.g. thorite, huttonite, thorianite, monazite, titanite, xenotime, allanite, zircon) host uranium and their alteration by acid hydrothermal or meteoric fluids is also a source of dissolved U in hydrothermal fluids or surface waters and groundwater; many uranium deposits are derived from them (Plant et al. 1999, Förster 1998, Gaines et al. 1997, Cabral Pinto et al. 2008, Hetherington and Harlov 2008).

The principal mechanism of dissolution of U from minerals is oxidation, and the oxidant is Fe^{III} (Abdelouas et al. 1999), which is produced by the oxidation of pyrite, usually found

associated with the uranium minerals. The uranyl ion (UO_2^{2+}) and its complexes are soluble in water and can be transported over distances up to kilometres. Changes in aqueous chemistry (pH, Eh, ionic potencial), temperature, and pressure lead to the precipitation of new uranium minerals, such as uranyl oxyhydroxides, carbonates, silicates, phosphates, vanadates, molybdates, arsenates, etc. (KOTZER and KYSER 1993, GAINES et al. 1997, FINCH and MURAKAMI 1999, MURPHY and SHOCK 1999, CABRAL PINTO et al. 2008). Uranyl ion can also be sorbed onto Fe oxyhydroxides (TRIPARTHI 1983, HSI AND LANGMUIR 1985, MURAKAMI et al. 1997, LOTTERMOSER AND ASHLEY 2005). Under reducing conditions U^{4+} precipitates as an insoluble UO_2 phase.

Uranium mineralizations are widespread in Central Portugal and some of them have been exploited, with interruptions, until the eighties, but nowadays the production is stopped. Although the uranium mines are of small size, the Portuguese uranium resources made Portugal the third or forth country with major resources in the Ocidental Europe (MATOS DIAS 1982). The Portuguese uranium deposits are mostly uranium-quartz veins related to uranium-bearing Variscan granites, which cut the granites and their contact metamorphic aureole. The structural control of the mineralizations is of extreme importance and locally the epithermal uranium mineralization overlays a sulphide mesothermal mineralization or a cassiterite-wolframite hypothermal mineralization (COTELO NEIVA 2003, CABRAL PINTO et al. 2008).

There are various generations of uraninite in the Portuguese uranium deposits. Coffinite is a reduced U-mineral contemporaneous with the last generation of uraninite (COTELO NEIVA 2003). The Portuguese uranium deposits also contain U^{6+} mineral species like oxides, phosphates, silicates, sulphates and arsenates (PAGEL 1981, COTELO NEIVA 2003, CABRAL PINTO et al. 2008).

The abandoned Vale de Abrutiga uranium mine, located in Central Portugal close to a Variscan peraluminous biotite granite, is an uranium phosphate mine, which was exploited until 1989. The granite has a mean of 10 ppm U, presents hydrothermal alteration and is the most probably source of U (CABRAL PINTO et al. 2008). The granite contains uraninite and thorite, while coffinite is also present in the hydrothermally altered granite. These minerals do not occur in the mineralized quartz veins. The ore mineral is saleeite, meta-saleeite and other U-phosphate phases, with similar compositions to saleeite but with different H_2O concentrations, which occur as aggregates of lamellar crystals in millimetre-sized veins.

The petrography and geochemistry of U-bearing minerals and phases from Vale de Abrutiga uranium mine were already given (CABRAL PINTO and SILVA 2007, CABRAL PINTO et al. 2008). The contamination associated with this uranium deposit was studied (PINTO et al. 2004). Besides uraninite, coffinite, thorite, some uranium-bearing minerals and mineral phases also occur in the granite and in the mineralized quartz veins. A systematic study using scanning electron microscopy, and obtaining X-ray maps and many new electron microprobe analyses of the uranium minerals (uraninite, coffinite, thorite, saleeite, meta-saleeite) and uranium-bearing minerals (xenotime, monazite, apatite, zircon, chlorite and anatase) is now presented. The samples are from the unaltered biotite granite, hydrothemally altered biotite granite and related hydrothermally uranium quartz veins. This study pretends to understand the release of U from minerals in the granite, its migration within the hydrothermal fluids, sorption and (re)precipitation in the mineralized quartz veins, under oxidizing conditions.

GEOLOGICAL SETTING

The coarse- to very coarse-grained porphyritic biotite Variscan granite (308±11 Ma, SILVA et al. 2000) is located in central Portugal and forms the border of the Beiras batholith. The granitic magma intruded the Cambrian Beira schist-metagraywake complex (Figure 1), which consists of chlorite phyllite with intercalations of metagraywake, metasandstone and metaconglomerates and minor thin marble and dolomitic marble beds. The intrusion produced an outer zone of contact metamorphism, consisting of mica schist, and an inner zone of discontinuous hornfels contact metamorphic aureole. Close to the contact, the granite shows a plane-linear fabric due to the N-S to 10°E orientation of feldspar phenocrysts caused by magmatic flux, NE-SW and also some NW-SE aplite, aplite-pegmatite and pegmatite veins and numerous quartz veins cut the granite.

The biotite granite is peraluminous and contains feldspar phenocrysts on average of 2 x 5 cm, but reach 10 x 15 cm and have euhedral, 1 x 1.5 cm, greenish blue cordierite, which is abundant close to the contact with the country rock. The granite also contains microgranular enclaves and xenoliths. The granite is hydrothermally altered if affected by faults and shear zones, and the altered zone is locally very deep.

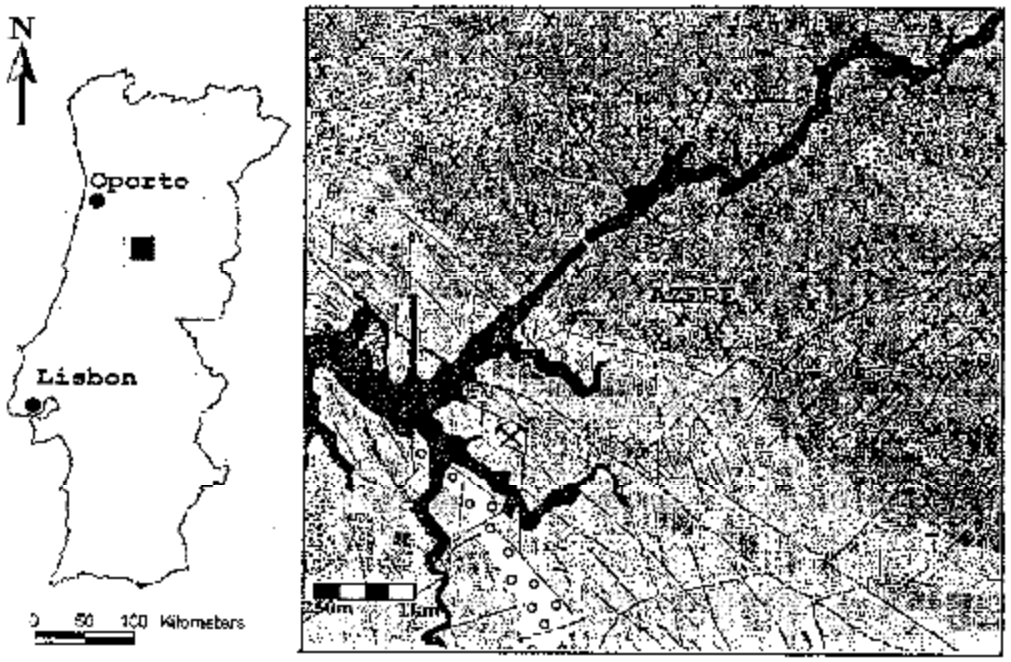

Figure 1. Location and geological map of the Variscan granite and related mineralized hydrothermal quartz veins. Modified from Cabral Pinto et al. (2008).

The uranium quartz veins cut the country phyllites, are thin, brecciated, aligned along the N45°W direction, which is the orientation of phyllite flux cleavage and contact granite-

country rock. They fill old NW-SE faults (Figure 1). The U-mineralization consists of secondary U-phosphates, mainly saleeite and meta-saleeite, occurs in the interception of this fault system with late N10-25°W faults, but also occurs disseminated in the phyllite at vein walls. The epithermal uranium mineralization of quartz veins overlays a hydrothermal wolframite-sulphide mineralization and the paragenetic sequence is given by CABRAL PINTO et al. (2008).

The abandoned Vale de Abrutiga uranium mine is located in the phyllites, close to the granite (Figure 1). It produced a total of 93,325 Kg U_3O_8, with a grade of 1kg U_3O_8/ton and operated from 1982 until 1989, with an interruption from 1983 to 1984 (ENU). The mineralization was disseminated from surface to about 50 m, and the exploration was an open pit.

ANALYTICAL METHODS

The unaltered granite was collected in quarries, but hydrothermally altered granite was obtained from altered areas. Samples from the mineralized quartz veins were collected in drill cores, provided by the National Uranium Enterprise (ENU).

The mineralogical characteristics were examined using reflected and transmitted light microscopy, secondary electron imaging (SEI), and backscattered electron imaging (BSE), in an electron microprobe. The electron microprobe analysis were performed on polished thin sections using two electron-microprobes, a JEOL JX8600 at the Department of Earth Sciences, University of Bristol, U.K., and a JEOL 8500-F, at LNEG, S. Mamede de Infesta, Portugal. The operating conditions for the JEOL JX8600 are given in CABRAL PINTO et al. (2008). The quantitative analysis and X-ray dot maps performed with the JEOL 8500-F were obtained with the five wavelength Spectrometers installed. Operating conditions were 20 kV accelerating voltage and 100 nA current. Beam diameter was kept at 1 μm. Counting times varied between 20 s for F, Si, Fe, P, Al, Ca and 60 s for Ce, La, Hf, Zr, Pb, Dy, Pr, Nd, Y, Ho, Er, Sm, Lu, Gd, Yb, Th and U in order to improve statistics and count rates. Detection limits obtained for REE elements range between 124 ppm and 252 ppm. The elements, standards and lines used are: Si ($Fe_3Al_2Si_3O_{12}$,Kα); Dy (DyP_5O_{14}, Lα); Fe (Fe_2O_3, Kα); F (CaF, Kα); P ($Ca_5(PO_4)_3F$, Kα); Hf (Hf, Lα); Pb (PbS, Lα); Al (Al_2O_3, Kα); Ca ($Ca_5(PO_4)_3F$, Kα); Pr (PrP_5O_{14}, Lβ); Ce (CeP_5O_{14}, Lα); Ti (TiO_2, Kα); Nd (NdP_5O_{14}, Lα); La (LaP_5O_{14}, Lα); Y (YAG, Lα); Ho (HoP_5O_{14}, Lα); Th (ThO_2, Mα); Er (ErP_5O_{14}, Lα); U (UO_2, Mβ); Sm (SmP_5O_{14}, Lα); Zr ($ZrSiO_4$, Lα); Lu (LuP_5O_{14}, Lα); Gd (GdP_5O_{14}, Lα), Yb (YbP_5O_{14}, Lα). The concentrations of Dy, Hf, Pr, Nd, Ho, Er, Sm, Lu, Gd and Yb were analysed using a LiFH crystal, mounted is a spectrometer which uses a smaller diameter Rowland Circle allowing higher count rates although poorer resolution of wavelength. Tb, Tm and Eu were not measured with this microprobe. Data reduction was made by the use of Armstrong method, which equips Jeol microprobes. X-ray lines and background offsets were carefully selected in order to minimize interferences and also necessary corrections. Overlapping peaks and backgrounds were identified after individual wavelength spectral scans on standards and specimens. The percentage of overlap was first determined by the calculation routine performed by the machine on the chosen standards. The interference of ThMβ on UMα and

YMα on Pb Mβ were eliminated by the use of ThMα UMβ and PbLα. Also the interference of LaLβ in Pr Lα was eliminated by the use of PrLβ.

PETROGRAPHY

Granite

The unaltered porphyritic, biotite Variscan granite contains quartz, microperthitic microcline, plagioclase, biotite, cordierite, rare primary muscovite, tourmaline, apatite, zircon, monazite, xenotime, uraninite, thorite, fluorite, ilmenite, rutile, pyrite and rare native gold and silver. It contains phenocrysts of microperthitic microcline and andesine-oligoclase (SILVA AND NEIVA, 1999/2000). The altered biotite granite contains the same minerals and also has secondary muscovite, chlorite, titanite, calcite, very rare epidote, allanite, coffinite, thorite and monazite.

Quartz is anhedral, with slight undulatory extinction and contains inclusions of feldspars, micas, monazite, xenotime, uraninite, coffinite, thorite, rutile and pyrite (Figure 2a, b). There are several generations of quartz. Quartz from altered granite is strongly fractured and frequently filled by alteration minerals (Figure 2b).

The petrography and chemistry of the major rock-forming minerals in the unaltered biotite granite is presented in SILVA AND NEIVA (1999/2000) and SILVA et al. (2000). Plagioclase has inclusions of biotite, muscovite, zircon, monazite, ilmenite, pyrite, uraninite, and thorite (Figure 2c). In the altered granite, both feldspars are vacuolated, fractured (Figure 2d), altered to secondary muscovite, and plagioclase is also altered to calcite.

Biotite contains inclusions of zircon, apatite, monazite, xenotime, ilmenite, pyrite, uraninite and thorite (Figure 2 e-h). Locally biotite occurs intergrowth with primary muscovite. In the altered granite, biotite is altered to chlorite. Titanite occurs related with this chloritization. Primary muscovite is subhedral and much less abundant than biotite. Muscovite contains quartz, zircon, apatite, monazite and xenotime inclusions. Cordierite is euhedral and generally do not contain inclusions in the unaltered granite. In the altered granite, cordierite is altered to a mixture of secondary muscovite and chlorite.

Tourmaline replaces feldspars and micas; is euhedral to anhedral, pleochroic from ω-pale yellow to ε- greenish yellow. The euhedral crystals are slightly zoned with a green rim and a light bluish green core. Crystal's dimensions are in average 0.5 mm x 3 mm and locally show zircon inclusions.

Uraninite occurs in the unaltered and altered granites, but it is rare in the altered granite. Uraninite crystals are small (5-10 μm) and occur enclosed in quartz, feldspar, micas, ilmenite, chlorite and apatite (Figure 2a, d, h). Uraninite is commonly associated with pyrite, zircon and monazite and produced radioactive damage halos. Euhedral crystals are restricted to the unaltered granite and nearly homogeneous uraninite largely predominates over zoned grains; back-scattered electron imaging did not reveal zonation (Figure 2h). In the altered granite, uraninite is fractured and vacuolated (Figure 2i-k) and the radioactive damage halos are filled with late pyrite, U-S-bearing phases and Fe oxyhydroxides (Figure 2k-m).

Coffinite occurs in the altered granite, enclosed in quartz. Coffinite crystals are anhedral to subhedral and have dimensions of 40 μm x 50 μm. Crystals are corroded and vacuolated; a

compositional heterogeneity core-rim within single crystals is clearly visible under backscattered electron (BSE) imaging (Figure 2n) and X-ray element mapping, where the altered rims of the crystals are relatively darker than unaltered areas. Some coffinite grains replace uraninite crystals (Figure 2i).

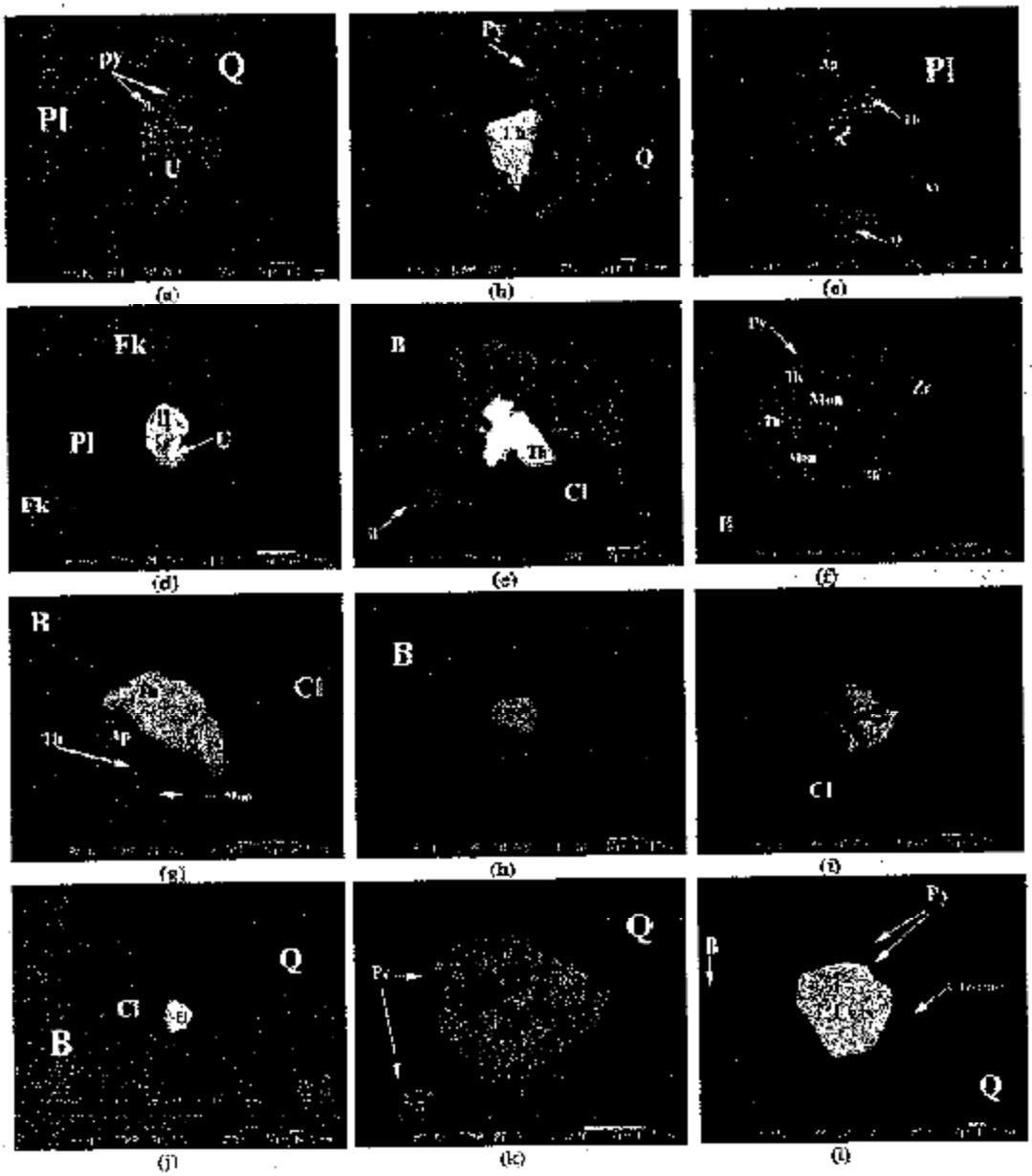

Figure 2. Backscattered images of minerals from the Variscan granite and related mineralized hydrothermal quartz veins, Central Portugal. Symbols: Al: allanite, Ap: apatite, B: biotite, Ca: calcite, Cl: chlorite, Cof: coffinite, Ep: epidote, Fe: Fe oxyhydroxides, Fe-U: U-bearing Fe oxyhydroxides, FK: K-feldspar, il: ilmenite, M: muscovite, Mon: monazite, Py: pyrite, Pl: plagioclase, Ph: Pb oxide, Q: quartz, S: saleeite, meta-saleeite and Fe-saleeite, Th: thorite, U: uraninite, U-Fe-phase: U-Fe bearing phases, Xe: xenotime, Z: zircon. (Continued on following pages)

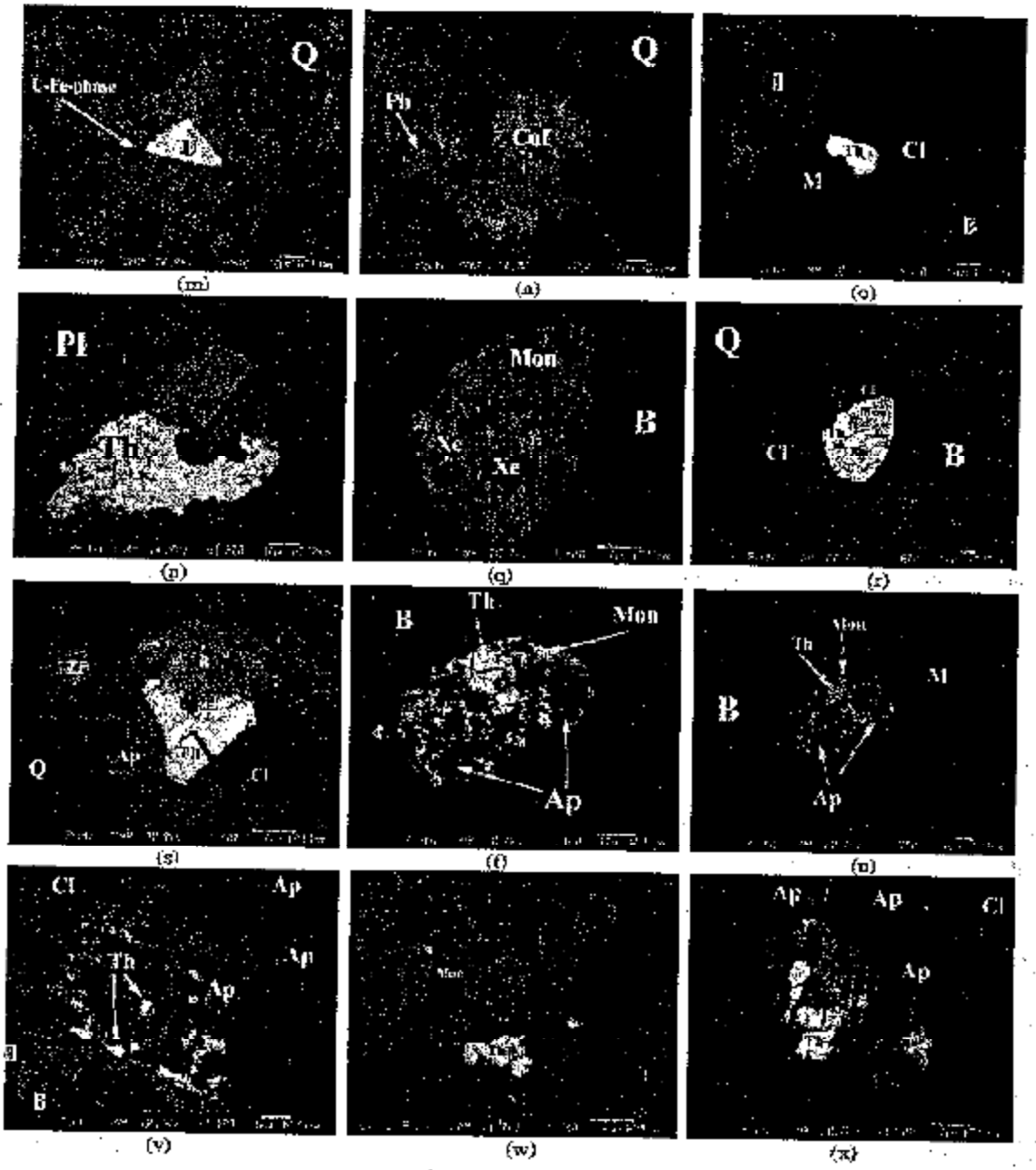

Figure 2 – continuation.

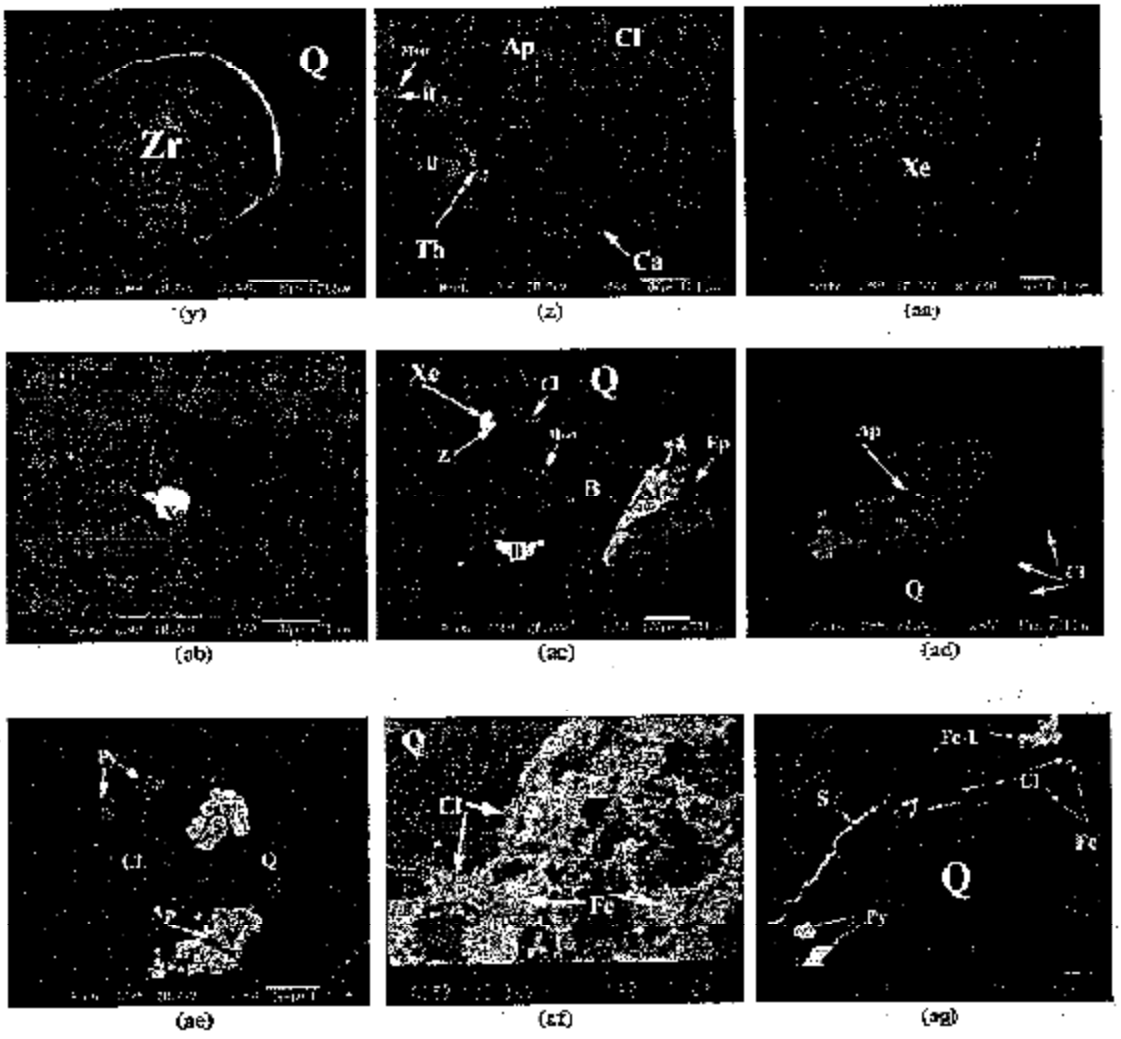

Figure 2 – continuation.

Photographies from the Variscan altered granite (photography (h) is from the unaltered granite):

(a) Crystal of uraninite (U) enclosed in quartz (Q) grain, with the radioactive damage zone filled with pyrite (Py).

(b) – Subhedral crystal of thorite (Th) with the radioactive damage zone filled with late pyrite (Py). Thorite is enclosed in fractured quartz (Q) grains.

(c) Fractured crystal of apatite (Ap), replaced by thorite (Th), enclosed in plagioclase (Pl).

(d) – Small crystal of uraninite (U) enclosed in ilmenite (il), which is enclosed in vacuolated plagioclase (Pl).

(e) – Anhedral crystal of thorite (Th) rimmed by pyrite (Py) and in contact with chlorite (Cl).

(f) – Monazite (Mon) rimmed by thorite (Th), which is rimmed by pyrite (Py). Monazite is associated with zircon (Zr), which is also in contact with thorite. Minerals are enclosed in biotite (B).

(g) – Apatite (Ap), replaced by monazite (Mon), which is replaced by thorite (Th), enclosed in biotite (B), and chloritized (Cl) biotite (B).

(h) – Small crystal of uraninite (U) enclosed in biotite (B) in the unaltered granite.

(i) – Fractured and zoned crystal of uraninite (U) enclosed in chlorite (Cl).

(j) – Crystal of uraninite (U) enclosed in fractured quartz (Q).

(k) – Fractured crystal of uraninite (U) enclosed in quartz (Q) grain, with the radioactive damage zone filled with pyrite (Py).
(l) – Crystal of uraninite (U), rimmed by a radioactive damage halo filled with U-Fe-S-bearing phases (U-Fe-phases) and pyrite (Py), enclosed in quartz (Q).
(m) – Crystal of uraninite (U), rimmed by a radioactive damage zone filled with U-Fe-bearing phases (U-Fe-phases) and pyrite (Py), enclosed in quartz (Q).
(n) – Corroded crystal of coffinite (Cof) enclosed in fractured quartz (Q), associated with an Pb oxide.
(o) – Anhedral crystal of thorite (Th) cutting chlorite (Cl) and muscovite (Ms).
(p) – Anhedral crystal of thorite (Th) associated with zircon (Zr), both enclosed in vacuolated plagioclase (Pl).
(q) – Fractured crystal of monazite (Mon), replaced by thorite (Th) and xenotime (Xe), enclosed in chloritezed (Cl) biotite (B).
(r) – Reduction of the photography (q): fractured crystal of monazite (Mon), replaced by thorite (Th) and xenotime (Xe), enclosed in chloritezed (Cl) biotite (B), which is in contact with quartz (Q).
(s) – Fractured crystal of apatite (Ap), replaced by thorite (Th), which is cutted by ilmenite (il), enclosed in fractured quartz (Q), and in contact with chlorite (Cl).
(t) – Fractured crystal of apatite (Ap), replaced by monazite (Mon), which is replaced by thorite (Th), enclosed in biotite (B).
(u) – Reduction of the photography (t): fractured crystal of apatite (Ap), replaced by monazite (Mon), which is replaced by thorite (Th), enclosed in biotite (B), which is in contact with muscovite.
(v) – Fractured crystal of apatite (Ap), replaced by monazite (Mon), which is replaced by thorite (Th) rimmed by ilmenite (il).
(w) – Fractured crystal of monazite (Mon) replaced by thorite (Th), enclose in chlorite (Cl).
(x) – Fractured crystal of apatite (Ap), replaced by monazite (Mon), which is replaced by thorite (Th), enclosed in chlorite (Cl).
(y) – Zoned crystal of zircon (Zr), enclosed in quartz (Q).
(z) – Fractured crystal of apatite (Ap), enclosed in chlorite (Cl), replaced by thorite (Th) in association with ilmenite (il). The apatite crystal is rimmed by calcite (Ca).
(aa) – Fractured crystal of xenotime (Xe).
(ab) – Reduction of the photography (aa): Fractured crystal of xenotime (Xe), cut by zircon, and cutting biotite (B) and plagioclase (Pl).
(ac) – Crystal of biotite (B), enclosed in quartz (Q), with the rims replaced by allanite (Al) associated with epidote (Ep) and chlorite (Cl). Xenotime (Xe) and zircon (Zr) are enclosed in biotite, and ilmenite (il) rims the biotite crystal.

Photographies from the related hydrothermal mineralized quartz veins:
(ad) – Uranium phosphates (S) replacing apatite (Ap), filling quartz (Q) fractures.
(ae) – Uranium phosphates (S) and pyrite (Py) filling quartz (Q) fractures.
(af) – Uranium phosphates (S), filling fractures in the mineralized quartz (Q) veins, associated with U-rich Fe oxyhydroxides (Fe-U) and pyrite (Py).
(ag) – Chlorite (Cl) weathered to Fe oxyhydroxides (Fe).

Thorite was found in all granite samples, however it occurs mainly in the altered granite. It occurs typically as small (5-8 μm) crystals; most of them are anhedral to subhedral (Figure 2b, c, e, g), some grains are strongly zoned (Figure 2o), and the within-grain compositional variability is large. It is usually hosted in major minerals of the granite, including quartz, biotite, muscovite, chlorite, apatite, plagioclase (Figure 2b, c), locally associated with zircon (Figure 2p), and locally cuts chlorite and muscovite (Figure 2o). In the altered granite, thorite fills fractures of other minerals, such as apatite, monazite and biotite (Figure 2s-x), mainly in their rims (Figure 2e, g, r, v) and seems to replace monazite along fractures, associated with xenotime (Figure 2q).

Zircon is zoned in the granite and enclosed in biotite and apatite and have inclusions of quartz. It is light brown to colourless, presents a very weak pleochroism, and is mainly euhedral and subhedral (Figure 2y), with variable dimensions, from 10 μm x 10 μm to 40 μm x 70 μm. Apatite is euhedral and subhedral. Its crystals are frequently fractured and have variable dimensions, from 200 μm x 300 μm to 20 μm x 30 μm. It occurs mainly enclosed in biotite and plagioclase (Figure 2c, u) and contains inclusions of zircon and uraninite. In the altered granite, crystals of apatite have a pervasive porosity, indicating dissolution of apatite with the formation of calcite (Figure 2z). It is also highly fracturated and is replaced by monazite and thorite (Figure 2z). Where alteration is more extensive, apatite is practically pseudomorphosed by thorite.

Xenotime occurs as euhedral, zoned, fractured crystals (~ 10 μm x 12 μm), enclosed in quartz and muscovite, associated with zircon (Figure 2aa, ab), and locally seems to cut micas and plagioclase (Figure 2ab). As referred above it also occurs associated with thorite where it is anhedral. Allanite occurs associated with epidote and chloritized biotite (Figure 2aa) in the altered granite. The crystals are anhedral and are mostly 50 to 100 μm in size, rarely up to 150 μm.

Ce-monazite is very light yellow, presents a very weak pleochroism, and commonly is hosted in biotite and plagioclase. In general, it occurs as subhedral crystals (15μm x 15μm), but in the altered granite the grains (15μm x 10μm) are anhedral, corroded, fractured and contain a scattering of holes or tiny inclusions of quartz. Locally it replaces apatite and is replaced by thorite (Figure 2t, u), which also occurs along its fractures. The altered monazite, close to the thorite, developed a high porosity and a distinct interface could be observed between the altered and the unaltered zones in monazite (Figure 2q).

Mineralized Quartz Veins

The petrography and the paragenetic sequence of the mineralized quartz veins from the Vale de Abrutiga were already published (Cabral Pinto and Silva 2007, Cabral Pinto et al. 2008); so only a summary of the petrographic characteristics of U-bearing minerals and associated minerals is presented. The hydrothermal quartz veins are brecciated and composed of quartz, muscovite, chlorite, pyrite, apatite, Fe oxyhydroxides, saleeite, meta-saleeite and other U-phosphate phases. Their accessory minerals are monazite, zircon, xenotime, ferberite, hübnerite, pyrrhotite, arsenopyrite, sphalerite and Ti oxides. The paragenetic sequence has three phases. The first phase consists of silicates, phosphates, oxides and sulphides. Silicates dominate in the second phase. The third phase consists mainly of Fe-oxides and U-phosphates that precipitated from late supergenic solutions (Cabral Pinto et al. 2008).

Quartz is anhedral and fractured, with muscovite, chlorite, pyrite, Fe oxyhydroxides and U-phosphates filling the fractures (Figure 2ad-ag). There are several generations of quartz. Xenotime is rare, small and occurs between, or enclosed in, the second and third generations of quartz or enclosed in the U-phosphates, and is associated with zircon. There are also several generations of pyrite and the last surrounds U-phosphates.

Zircon is anhedral to subhedral with dimensions bigger than in the granite (up to 50 μm x 120 μm) and is generally enclosed in quartz. Zoned, dissolved and fractured zircon grains were found and the fractures are filled with quartz and Fe oxyhydroxides. Apatite is rare,

subhedral and is always dissolved and replaced by U-phosphates (Figure 2ad, ae). Its dimensions range from 10 μm x 10 μm to 100 μm x 150 μm. Monazite occurs enclosed in quartz, muscovite, Fe oxyhydroxides and also between quartz crystals. It is anhedral, bigger than in the granite (average dimension is 25 μm x 40μm), frequently dissolved and some of its vacuoles are filled with quartz.

Muscovite and chlorite also occur in several generations; locally they are intergrown, surrounded by U-bearing Fe oxyhydroxides and in contact with saleeite and meta-saleeite. Chlorite is weathered to Fe oxyhydroxides (Figure 2af). Ti oxides (anatase) are dark reddish brown and the crystals are often dissolved and vacuolated and surrounded by uranium-rich Fe oxyhydroxides.

Fe oxyhydroxides are abundant in the mineralized quartz veins. They are reddish brown and reddish orange, often banded, locally show colloidal textures, fill fractures and microfractures, surround the other crystals, occur as masses, frequently replace muscovite, chlorite, Ti oxides and are surrounded by uranium phosphates.

Macroscopic crystals of U-phosphates occur in the mineralized quartz veins, and in the adjacent phyllite, forming millimetre-sized veins and locally they cut pyrite. Saleeite and meta-saleeite were not distinguished by EDS at the SEM. They are the last minerals, filling microfractures and the space between grain boundaries (Figure 2ag), have a yellowish and brownish colour, and occur as aggregates of lamellar crystals, mostly in the range 5 μm x 20 μm. They are often associated with pyrite, chlorite, surround the Fe-U oxyhydroxides and replace U-rich apatite.

Chemical Composition of U-Minerals and U-Bearing Minerals

Chemical analyses of uraninite are given in Table 1. The average chemical formula of uraninite from the unaltered granite is $U_{0.93}Pb_{0.05}Th_{0.02}Fe_{0.02}$ (Table 1). Thorium contents are low, and Pb is the second cation in uraninite (Table 1). The uraninite is poor in Y (mean concentrations of 0.006 a.p.f.u.) and REE [mean concentrations of ≤ 0.002 a.p.f.u. LREE (Ce+Pr+Nd+Sm) and of ≤ 0.001 a.p.f.u. HREE (Gd+Dy+Ho+Er+Yb+Lu)]. Silicium and Al were present with very low contents, of 0.007 a.p.f.u. and 0.002 a.p.f.u., respectively, (Table 1), but Si reaches 0.023 a.p.f.u., and Al is up 0.012 a.p.f.u. (Cabral Pinto et al. 2008). Calcium and Fe mean contents are 0.004 a.p.f.u. and 0.020 a.p.f.u., respectively. The analytical totals have a mean value of 98.84 wt.%. The crystals have rims richer in U and poorer in Th than cores (Table 1).

The average chemical formula of uraninite from the altered granite is $U_{0.90}Pb_{0.05}Th_{0.02}Fe_{0.03}$ and the analytical totals range from 93.0 to 97.7 wt.% (Table 1). Generally, the uraninite from the altered granite contains lower concentrations of U than uraninite from fresh samples, ranging between 0.874 and 0.926 a.p.f.u. and with a mean value of 0.903 a.p.f.u. The mean concentrations of Pb and Ca are also slightly lower than in unaltered uraninite (Table 1).

Table 1. Chemical compositions (in weigh percent) and structural formula of uraninite and coffinite from the unaltered and altered Variscan granites, Central Portugal

	Uraninite										Coffinite														
	Unaltered granite				Altered granite						Crystal A														
	Mean	σ	rim	core	Mean	σ	rim	core	1	2	rims		cores												
Al_2O_3	0.04	0.07	—	—	0.07	0.11	0.02	0.06	0.12	0.23	—	—	0.01	0.01	0.01	—	—	—	—	0.06	0.05	0.00	0.48	—	
SiO_2	0.14	0.16	0.19	0.17	0.51	0.40	0.07	—	0.21	0.17	16.89	14.97	16.82	15.34	15.32	16.73	16.79	16.97	17.30	14.91	13.97	14.85	16.16	17.88	
P_2O_5	0.03	0.03	0.01	0.02	0.01	0.01	0.03	0.02	—	0.03	—	0.33	0.02	0.02	0.02	0.02	0.02	0.01	—	0.04	0.03	0.05	—	—	
CaO	0.03	0.13	—	—	0.03	0.09	—	—	0.83	—	0.96	0.80	—	—	—	1.01	—	—	0.96	2.02	1.22	1.19	2.22	2.22	
ZrO_2	0.04	0.02	0.09	0.04	0.02	0.03	0.04	—	0.01	0.04	0.04	0.71	—	—	—	—	—	—	—	0.02	—	0.01	—	—	
HfO_2	0.02	0.05	0.01	0.14		—	—	—	—	0.01	—	—	—	—	—	—	—	—	—	—	0.05		—	—	
TiO_2	—	—	n.d.	n.d.	—	—	—	—	—	—	—	—	—		—	—	—	—	—	—	—	—	—	—	
Fe_2O_3	0.52	0.52	0.02	0.81	0.30	0.41	0.39	0.07	0.16	0.38	0.01	1.34	—	—	—	0.04	0.04	0.03	0.03	1.06	0.92	0.45	0.93	0.94	
Y_2O_3	0.25	0.14	0.42	0.41	0.40	0.10	0.22	0.01	0.19	0.22	0.00	0.00	—	—	—	—	—	—	—	0.40	0.37	0.43	—	0.97	
La_2O_3	0.01	0.02	—	—	—	0.01	—	—	0.01	—	—	—	—	—	—	—	—	0.01	0.01	0.00	0.07	—	—	—	
Ce_2O_3	0.08	0.09	0.07	0.11	0.06	0.04	—	0.04	0.03	0.04	0.10	0.15	0.08	0.07	0.08	0.02	0.02	0.02	—	0.23	0.19	0.25	—	0.07	
Pr_2O_3	—	—	—	—	—	0.01	—	—	—	—	0.04	—	0.04	—	0.04	—	—	—	—	—	—	—	—	—	
Nd_2O_3	0.02	0.03	—	—	0.05	0.03	—	—	0.03	0.06	—	—	—	—	—	—	—	—	—	—	—	—	—	—	
Sm_2O_3	0.01	0.01	n.d.	n.d.	0.01	0.02	—	—	0.02	—	—	—	—	—	—	—	—	—	—	n.d.	n.d.	n.d.	n.d.	n.d.	
Gd_2O_3	—	—	n.d.	n.d.	0.03	0.01	—	0.01	—	0.04	0.02	—	—	—	—	0.01	0.01	—	—	n.d.	n.d.	n.d.	n.d.	n.d.	
Dy_2O_3	0.04	0.01	n.d.	n.d.	0.0	0.03	0.01	0.01	0.05	0.05	0.03	—	—	—	—	—	—	—	—	n.d.	n.d.	n.d.	n.d.	n.d.	
Ho_2O_3	0.03	—	n.d.	n.d.	0.04	0.02	—	—	0.06	0.01	0.02	—	0.02	0.03	0.02	0.01	0.01	0.02	—	n.d.	n.d.	n.d.	n.d.	n.d.	
Er_2O_3	0.01	0.01	n.d.	n.d.	0.01	0.01	—	—	—	0.02	—	—	—	0.01	—	0.02	0.02	—	—	n.d.	n.d.	n.d.	n.d.	n.d.	
Yb_2O_3	—	—	n.d.	n.d.	0.02	0.02	—	—	—	—	—	—	—	—	—	—	—	—	—	n.d.	n.d.	n.d.	n.d.	n.d.	
Lu_2O_3	0.01	0.01	n.d.	n.d.	—	—	—	—	—	—	—	—	—	0.02	—	0.01	0.01	—	—	n.d.	n.d.	n.d.	n.d.	n.d.	
PbO	3.82	0.17	3.70	3.70	3.87	0.05	3.28	3.77	3.72	3.69	0.88	2.41	0.16	0.05	0.15	0.08	0.08	0.08	0.01	1.38	1.52	1.20	0.07	0.45	
ThO_2	1.57	0.55	1.28	3.01	1.51	0.83	0.73	0.08	0.81	0.87	1.88	3.15	—	—	—	—	—	—	0.03	1.24	1.24	1.21	—	—	
UO_2	91.08	1.76	92.03	89.99	92.57	1.31	86.72	90.16	89.72	89.72	70.62	64.89	81.66	85.95	81.65	72.55	72.55	77.82	72.07	60.00	70.91	70.02	75.12	75.15	
F	0.12	0.22	n.d.	n.d.	0.42	0.11	0.46	0.32	0.55	0.48	0.36	0.21	0.37	0.38	0.37	0.32	0.32	0.31	0.44	n.d.	n.d.	n.d.	n.d.	n.d.	
Total	98.84	1.40	97.78	98.50	98.82	1.30	91.85	95.46	95.83	95.10	91.43	88.75	98.15	96.84	98.18	92.83	93.02	92.58	93.90	120.73	95.54	98.97	98.10	97.64	
Al	0.002	0.004	—	—	0.004	0.006	0.001	0.003	0.005	0.012	—	—	—	0.001	—	—	—	—	—	0.004	0.004	0.005	0.031		
Si	0.007	0.007	0.009	0.008	0.023	0.016	0.003	—	0.010	0.008	0.805	0.818	0.921	0.828	0.821	1.040	1.009	0.884	0.883	0.824	0.959	0.851	0.985	0.803	
P	0.001	0.001	—	0.001	—	—	0.001	0.001	—	0.001	—	0.017	0.001	0.001	0.001	0.001	0.001	0.001	—	0.002	0.002	0.002	—	—	
Ca	0.006	0.005	—	—	0.001	0.005	—	—	0.018	—	0.060	0.052	—	—	—	0.061	—	—	0.060	0.126	0.078	0.079	0.130	0.131	
Zr	0.001	0.001	0.002	0.001	—	0.001	0.001	—		0.001	0.001	0.021	—	—	—	—	—	—	—	0.001	—	0.001	—	—	
Hf	—	0.001	—	0.002	—	—	—	—	—	—	—	—	—	—	—	—	—	—	—	—	0.001	—	—	—	
Ti	—	—	n.d.	n.d.	—	—	—	—	—	—	—	—	—	—	—	—	—	—	—	—	—	—	—	—	
Fe	0.020	0.023	0.001	0.035	0.011	0.016	0.018	0.003	0.005	0.016	—	0.059	—	—	—	0.002	0.002	0.002	0.001	0.052	0.046	0.023	0.000	0.002	
Y	0.009	0.004	0.010	0.010	0.010	0.002	0.005	—	0.005	0.005	0.003	0.025	—	—	—	—	—	—	—	0.014	0.012	0.014	—	0.015	
La	—	—	—	—	—	—	—	—	—	—	—	—	—	—	—	—	—	—	—	0.002	0.001	—	—	—	
Ce	0.005	0.001	0.001	0.002	0.001	0.001	0.001	—	0.001	0.001	0.002	0.005	0.002	—	0.002	0.001	0.001	—	—	0.005	0.004	0.005	—	0.001	
Pr	—	—	—	—	—	—	—	—	—	—	0.001	—	0.001	—	0.001	—	—	—	—	—	—	—	—	—	
Nd	—	0.001	—	—	0.001	0.001	—	—	—	0.001	—	—	—	—	—	—	—	—	—	—	—	—	—	—	
Sm	—	—	n.d.	n.d.	—	—	—	—	—	—	—	—	—	—	—	—	—	—	—	n.d.	n.d.	n.d.	n.d.	n.d.	
Gd	—	—	n.d.	n.d.	0.001	—	—	—	—	0.001	—	—	—	—	—	—	—	—	—	n.d.	n.d.	n.d.	n.d.	n.d.	
Dy	0.001	—	n.d.	n.d.	0.001	—	—	—	0.001	0.001	—	—	—	—	—	—	—	—	—	n.d.	n.d.	n.d.	n.d.	n.d.	
Ho	—	—	n.d.	n.d.	0.001	—	—	—	0.001	—	—	—	—	0.001	—	—	—	—	—	n.d.	n.d.	n.d.	n.d.	n.d.	
Er	—	—	n.d.	n.d.	—	—	—	—	—	—	—	—	—	—	—	0.001	0.001	—	—	n.d.	n.d.	n.d.	n.d.	n.d.	
Yb	—	—	n.d.	n.d.	—	—	—	—	—	—	—	—	—	—	—	—	—	—	—	n.d.	n.d.	n.d.	n.d.	n.d.	
Lu	—	—	n.d.	n.d.	—	—	—	—	—	—	—	—	—	—	—	—	—	—	—	n.d.	n.d.	n.d.	n.d.	n.d.	
Pb	0.047	0.002	0.048	0.048	0.045	0.001	0.043	0.048	0.048	0.045	0.011	0.040	0.002	0.001	0.003	0.001	0.001	0.002	—	0.012	0.008	0.020	0.001	0.007	
Th	0.010	0.008	0.013	0.031	0.010	0.009	0.010	0.001	0.008	0.013	0.023	0.044	—	—	—	—	—	—	—	0.010	0.017	0.010	—	—	

Table 2. Chemical composition (in weigh percent) and structural formula of thorite from the Variscan unaltered and altered granites, Central Portugal

Thorite — Unaltered granite

	1	2	3	4	5	6	7	8	9	10	11	12	13	14	15	Mean	σ
P_2O_5	3.98	4.80	8.22	6.11	0.52	4.00	4.25	6.58	0.77	1.34	3.47	2.88	2.78	1.19	0.04	3.01	2.28
SiO_2	16.55	15.18	14.83	14.49	7.37	15.08	14.89	7.77	17.69	17.39	12.81	16.29	14.29	16.28	19.87	14.49	3.13
TiO_2	0.33	0.19	2.36	0.19	3.13	0.05	0.02	0.31	n.d.	n.d.	n.d.	n.d.	n.d.	n.d.	n.d.	0.15	0.13
ZrO_2	—	0.35	0.68	0.41	—	5.07	0.60	—	0.25	—	0.31	0.81	—	—	0.10	0.41	0.25
HfO	0.05	0.02	0.08	0.04	-	0.03	0.48	—	—	0.04	0.04	—	0.05	—	0.02	0.04	0.02
ThO_2	46.75	55.06	44.95	59.71	66.31	59.72	54.09	57.38	63.30	64.99	60.75	61.58	46.54	48.82	54.05	54.00	4.88
UO_2	1.31	1.54	0.56	0.45	6.03	0.51	0.83	7.32	8.83	5.89	6.78	4.23	1.71	7.51	6.62	3.56	3.06
Al_2O_3	0.06	0.35	0.71	0.61	1.42	—	0.03	0.51	—		—		—	—	0.20	0.47	0.28
Y_2O_3	0.19	0.25	0.74	0.08	1.75	0.01	0.09	0.61	0.36	2.03	0.11	3.67	5.83	2.65	1.37	1.28	1.66
La_2O_3	0.05	0.25	0.50	0.47	—	3.18	0.04	—	—	0.17	0.10	0.23	0.02	0.24	0.18	0.33	0.25
Ce_2O_3	0.37	0.63	3.64	0.27	—	3.27	0.36	0.02	0.08	1.58	0.17	1.67	0.71	1.46	0.76	0.83	1.01
Pr_2O_3	0.28	0.11	0.45	0.09	—	3.07	0.06	—	—	—	—	—	—	—	—	0.12	0.17
Nd_2O_3	0.31	0.41	2.01	0.26	—	0.13	0.24	—	—	—	—	—	—	—	—	0.57	0.71
Sm_2O_3	0.07	0.04	0.13	0.01	0.07	—	0.01	—	n.d.	n.d.	n.d.	n.d.	n.d.	n.d.	n.d.	0.05	0.05
Gd_2O_3	0.00	0.14	0.77	0.66	0.07	0.04	0.03	0.03	n.d.	n.d.	n.d.	n.d.	n.d.	n.d.	n.d.	0.15	0.25
Dy_2O_3	0.80	0.51	0.72	0.63	0.55	0.50	0.60	0.50	n.d.	n.d.	n.d.	n.d.	n.d.	n.d.	n.d.	0.55	0.59
Ho_2O_3	0.58	0.81	0.10	—	0.03	0.01	0.01	—	n.d.	n.d.	n.d.	n.d.	n.d.	n.d.	n.d.	0.03	0.04
Er_2O_3	0.02	0.03	0.19	—	0.32	—	0.01	0.02	n.d.	n.d.	n.d.	n.d.	n.d.	n.d.	n.d.	0.04	0.08
Yb_2O_3	0.04	0.02	0.25	—	—	—	—	—	n.d.	n.d.	n.d.	n.d.	n.d.	n.d.	n.d.	0.08	0.08
Lu_2O_3	0.18	0.05	0.01	—	—	—	—	—	n.d.	n.d.	n.d.	n.d.	n.d.	n.d.	n.d.	0.04	0.05
FeO	0.46	1.24	0.07	2.42	1.33	1.02	0.38	1.39	0.24	1.81	2.35	1.81	2.09	0.47	0.86	1.14	0.76
CaO	2.00	1.27	3.39	1.60	1.86	1.05	2.63	1.33	2.11	1.45	2.09	2.09	1.58	1.36	1.97	1.82	0.36
PbO	0.27	1.75	0.74	3.20	3.28	2.21	2.03	0.78	0.12	0.05	0.95	0.29	0.10	0.06	0.12	0.79	1.03
F	0.27	0.15	0.18	0.24	0.68	0.25	2.40	1.02	n.d.	n.d.	n.d.	n.d.	n.d.	n.d.	n.d.	0.40	0.30
Total	78.97	84.40	93.67	91.28	75.49	88.21	87.50	78.91	83.87	85.17	81.42	85.10	77.56	80.55	83.01	84.36	4.06
P	0.192	0.217	0.360	0.280	0.036	0.104	0.302	0.042	0.035	0.051	0.178	0.135	0.144	0.058	0.042	0.147	0.057
Si	0.956	0.946	0.747	0.793	0.832	0.966	0.900	0.883	1.094	1.002	0.783	0.885	0.870	0.983	0.887	0.839	0.139
Ti	0.001	0.005	0.014	0.005	0.058	0.003	0.001	0.015								0.007	0.205
Zr	—	0.210	5.016	0.010	—	0.050	0.022	—	0.007		0.000	0.019	—	—	0.004	0.012	0.097
Hf	0.001	0.001	0.001	0.006		—	0.001	—	—	0.351	0.001	—	0.003	—	—	—	0.000
Th	0.845	0.687	0.818	0.715	1.309	0.778	0.708	0.877	0.711	0.735	0.837	0.625	0.672	0.673	0.723	0.710	0.120
U	0.025	0.019	0.007	0.018	0.103	0.007	0.305	0.137	0.112	0.076	0.010	0.053	0.023	0.101	0.087	0.049	0.045
Al	0.004	0.021	0.042	0.037	0.040	—	0.006	0.045	—	—		—	0.000	—	0.014	0.025	0.018
Y	0.027	0.007	0.020	0.002	0.032	—	0.059	0.024	0.018	0.069	0.204	0.110	0.163	0.207	0.040	0.046	0.083
La	0.001	0.005	0.047	0.009	—	0.029	0.001	—	—	0.026	0.002	0.005	—	0.105	0.002	0.006	0.055
Ce	0.008	0.011	0.067	0.006	—	0.006	0.008	0.031	0.002	0.039	0.064	0.014	0.017	0.032	0.017	0.018	0.018
Pr	0.006	0.002	0.009	0.002	—	0.001	0.001	—	—	—	—	—	—	—	—	0.024	0.003
Nd	0.009	0.028	0.038	0.026	—	0.003	0.005	—	—	—	—	—	—	—	—	0.012	0.013
Sm	0.001	0.021	0.002	—	0.001	—	—	—	n.d.	n.d.	n.d.	n.d.	n.d.	n.d.	n.d.	0.021	0.001
Gd	0.002	0.002	0.015	0.001	0.012	0.031	—	0.001	n.d.	n.d.	n.d.	n.d.	n.d.	n.d.	n.d.	0.003	0.004

Thorite — Crystal A (Fractured crystal) and Crystal B (Zoned crystal)

	Crystal A Unaltered Zone	Crystal A Unaltered Zone	Crystal A Altered Zone	Crystal A Altered Zone	Crystal B Core	Crystal B Rim
P_2O_5	2.38	1.77	7.55	5.25	0.80	3.87
SiO_2	16.45	16.03	4.08	12.90	16.97	15.33
TiO_2	—	—	0.02	1.21	0.14	0.03
ZrO_2	0.01	0.08	0.17	1.00	0.03	0.01
HfO	0.01	0.01	—	0.05	—	0.03
ThO_2	48.64	55.50	46.87	52.80	58.81	60.02
UO_2	10.43	7.23	3.87	0.40	3.63	0.77
Al_2O_3	0.69	0.04	3.42	0.48	0.42	0.01
Y_2O_3	0.40	0.40	3.17	0.14	0.51	0.07
La_2O_3	0.25	0.02	0.05	0.37	0.06	0.12
Ce_2O_3	0.10	0.10	0.36	0.28	0.16	0.22
Pr_2O_3	0.14	0.01	0.01	0.06	0.04	0.03
Nd_2O_3	3.52	0.71	0.03	0.25	0.04	0.13
Sm_2O_3	0.09	0.03	—	2.02	5.54	—
Gd_2O_3	0.33	0.03	0.06	0.64	2.15	0.09
Dy_2O_3	0.61	0.49	0.50	0.60	0.65	0.61
Ho_2O_3	—	—	—	—	0.02	0.01
Er_2O_3	0.03	0.01	0.01	0.02	—	—
Yb_2O_3	—	0.23	—	—	—	—
Lu_2O_3	0.33	—	—	—	—	—
FeO	0.47	0.34	4.16	1.69	0.78	1.09
CaO	2.57	0.35	3.30	2.45	2.10	1.08
PbO	0.62	0.01	1.35	2.77	0.61	2.59
F	0.16	0.05	1.48	0.33	0.09	0.20
Total	82.66	82.58	80.22	82.69	84.57	93.61
P	0.115	0.031	0.349	0.206	0.058	0.046
Si	0.942	0.973	0.619	0.746	1.020	0.858
Ti	—	—	0.001	0.008	0.015	0.001
Zr	—	0.003	0.004	0.025	0.001	—
Hf	—	—	—	0.001	—	0.001
Th	0.637	0.788	0.598	0.664	0.722	0.853
U	0.133	0.097	0.048	0.026	0.047	0.011
Al	0.046	0.001	0.027	0.032	0.026	—
Y	0.012	0.003	0.005	0.004	0.024	0.022
La	0.006	—	0.001	0.004	0.001	0.003
Ce	0.032	0.022	0.008	0.006	0.019	0.005
Pr	0.002	0.002	—	0.001	0.001	0.001
Nd	0.011	0.005	0.012	0.009	0.052	0.053
Sm	0.002	—	—	—	0.061	—
Gd	0.007	0.005	0.001	0.001	0.005	0.001

Thorite — Altered granite

	1	2	3	4	5	6	7	8	9	10	11	Mean	σ
P_2O_5	8.47	3.36	3.51	7.21	4.78	4.12	1.30	1.77	1.67	4.32	2.44	4.45	2.78
SiO_2	8.18	13.05	13.84	18.57	14.35	16.31	17.22	16.78	18.57	11.42	13.48	14.57	2.77
TiO_2	0.29	0.21	0.30	0.21	0.27	—	0.02	n.d.	n.d.	n.d.	n.d.	0.17	0.10
ZrO_2	0.56	4.82	5.93	5.81	0.32	0.10	—	—	0.14	2.38	0.50	1.42	2.16
HfO	0.02	0.56	0.16	0.23	0.02	0.01	—	—		0.09	3.04	0.05	0.07
ThO_2	60.37	46.55	38.97	43.01	58.58	53.76	47.61	62.63	56.78	50.14	57.64	54.16	7.57
UO_2	1.41	0.78	1.16	1.20	0.54	0.87	6.50	6.80	5.93	0.81	1.06	2.76	2.82
Al_2O_3	1.10	0.31	0.96	0.67	0.55	0.08	0.25	0.99	3.43	2.34	0.47	0.49	0.33
Y_2O_3	0.99	3.81	4.13	4.20	0.33	0.48	1.16	1.45	1.25	0.33	0.68	1.11	1.46
La_2O_3	0.14	0.98	1.01	1.11	0.23	0.09	0.17	0.10	0.07	0.03	0.09	0.29	0.37
Ce_2O_3	0.51	3.65	3.30	3.33	0.13	0.07	0.79	1.32	1.54	0.87	0.55	0.54	1.72
Pr_2O_3	0.03	1.52	0.37	3.43	0.02	0.10	0.15	—	—	—	—	0.15	0.18
Nd_2O_3	0.37	2.61	2.11	2.46	0.18	0.60	0.92	—	—	—	—	0.76	0.93
Sm_2O_3	—	0.11	0.27	0.14	0.41	0.14	0.06	n.d.	n.d.	n.d.	n.d.	0.09	0.08
Gd_2O_3	0.07	0.70	0.95	0.86	0.04	0.25	0.30	n.d.	n.d.	n.d.	n.d.	0.30	0.33
Dy_2O_3	0.98	1.23	1.36	1.22	0.90	0.72	0.31	n.d.	n.d.	n.d.	n.d.	0.71	0.37
Ho_2O_3	—	0.11	0.08	0.10	—	—	—	n.d.	n.d.	n.d.	n.d.	0.38	0.05
Er_2O_3	—	0.21	0.17	2.14	0.05	0.07	0.01	n.d.	n.d.	n.d.	n.d.	0.07	0.08
Yb_2O_3	—	0.20	0.20	3.22	—	0.04	-	n.d.	n.d.	n.d.	n.d.	0.14	0.10
Lu_2O_3	—	0.02	0.06	0.07	—	—	—	n.d.	n.d.	n.d.	n.d.	0.35	0.03
FeO	1.19	0.66	0.64	0.50	2.55	0.48	0.34	0.34	2.92	2.22	1.24	1.26	1.09
CaO	9.65	3.43	9.01	3.85	1.55	4.01	1.54	2.14	2.09	2.66	1.54	2.52	1.07
PbO	0.12	0.53	0.20	0.22	9.02	0.05	0.19	0.09	0.50	0.17	9.28	0.82	1.07
F	0.50	5.06	1.58	0.65	0.67	0.01	0.00	n.d.	n.d.	n.d.	n.d.	0.41	0.55
Total	89.54	83.30	93.28	84.77	86.83	82.34	76.71	88.88	86.93	85.88	82.20	87.98	5.56
P	0.977	0.382	0.365	0.207	0.221	0.182	0.068	0.047	0.050	0.235	0.125	0.262	0.115
Si	0.430	0.668	0.640	0.733	0.783	0.696	1.051	1.017	0.945	0.858	0.925	0.787	0.179
Ti	0.059	0.008	0.010	0.307	0.011	—	0.024	n.d.	n.d.	n.d.	n.d.	0.007	0.004
Zr	0.014	0.110	0.125	0.118	0.314	0.203	—	—	0.304	0.097	0.009	0.037	0.041
Hf	—	0.031	0.072	0.008	—	—	—	—	—	0.004	0.001	0.021	—
Th	0.624	0.400	0.393	0.430	0.719	0.673	0.658	0.790	0.723	0.751	0.788	0.660	0.133
U	0.018	0.508	0.011	0.072	0.007	0.012	0.577	0.010	0.075	0.010	0.121	0.031	0.036
Al	0.058	0.017	0.050	0.434	0.041	0.004	0.071	0.081	0.025	0.023	0.035	0.031	0.018
Y	0.079	0.055	0.065	0.038	0.102	0.314	0.005	0.042	0.068	0.026	0.022	0.032	0.034
La	0.001	0.017	0.016	0.018	0.306	0.005	0.004	0.002	0.052	0.001	0.004	0.056	0.005
Ce	0.012	0.062	0.051	0.054	0.004	0.001	0.015	0.025	0.013	0.014	0.012	0.018	0.02
Pr	0.001	0.005	0.005	0.018	—	0.002	0.003	—	—	—	—	0.023	0.003
Nd	0.003	0.042	0.033	0.036	0.004	0.012	0.011	—	—	—	—	0.014	0.015
Sm	—	0.002	0.004	0.002	—	0.003	0.001	n.d.	n.d.	n.d.	n.d.	0.002	0.001
Gd	0.001	0.011	0.014	0.019	0.001	0.005	0.006	n.d.	n.d.	n.d.	n.d.	0.009	0.002

—: not detected. n.d.: not determined. Cation formula based on four atoms of oxygen for thorite.

Thorium (of < 0.031 a.p.f.u.), Y (of ≤ 0.011 a.p.f.u.), LREE (of ≤ 0.002 a.p.f.u.) and HREE (of ≤ 0.003 a.p.f.u.) contents are similar in uraninite from unaltered granite and altered granite. Altered uraninite, from the altered granite, has higher mean Si, and F (0.023 and 0.060 a.p.f.u., respectively) concentrations than unaltered uraninite (0.007 a.p.f.u. Si and 0.017 a.p.f.u. F). Mean Fe concentration of uraninite is lower in the altered granite than in the unaltered granite (0.011 and 0.020 a.p.f.u., respectively). Therefore, in general uraninite from the altered granite is poorer in U, Fe, Pb, Ca and richer in Si and F. Locally, in the altered samples, uraninite is replaced by coffinite (Figure 2f) and it has lower Th and Y and similar U contents to uraninite from the altered samples (Table 1, analyses 1 and 2).

In spite of the small dimensions of uraninite grains, we can observe pattern zonings by X-ray dot map obtained by the electron microprobe. Altered areas of uraninite crystals are relatively darker than unaltered areas, which is due to a relatively lower U content. In the altered granite, the uraninite grains have lower U contents in the rims than in the cores and, generally, rims and alteration zones are poorer in U, Th, Pb and Ce than cores (Table 1, Figure 3a).

Representative data for the chemical composition of coffinite from altered granite are given in Table 1. The characteristic feature of this coffinite is relatively variable concentrations of Si (0.824-1.049 a.p.f.u) and U (0.886-1.095 a.p.f.u). The amounts of Ca range from below the detection limit to 0.131 a.p.f.u. The coffinite is poor in Y, P, and REE, particularly in HREE, with concentrations of Y ≤ 0.023 a.p.f.u., P ≤ 0.017 a.p.f.u., (La+Ce+Pr+Nd+Sm) ≤ 0.007 a.p.f.u. and (Gd+Dy+Ho+Er+Yb+Lu) ≤ 0.001 a.p.f.u. Thorium and Pb contents are low reaching 0.044 a.p.f.u. and 0.040 a.p.f.u., respectively. The analytical totals range from 89.75 to 100.73 wt.%, probably due to different degrees of hydratation (Table 1).

Backscattered electron (BSE) images and X-ray element maps show clearly differences between rims and cores of coffinite, reflecting an enrichment in Th, Ca, Pb, Zr and an impoverishment in U in the crystal rims (Table 1, Figure 3b). Coffinite intergrowths with thorite were not found, but some coffinite grains replace uraninite (Figure 2f).

Thorite was found in all the granite samples and its composition is very variable in all of them, even within the grains. This variability is also referred by Forster (2006). Thorite occurs as very fine-grained crystals (~10 μm), forms intergrowth with large amounts of associated minerals, such as xenotime, monazite, apatite and zircon (Figs 2e, e-g, p-w). The composition of thorite is dominated by the major components Th and Si. Thorium concentrations of thorite range between 44.95-60.75 wt.% ThO_2 in the unaltered granite, and between 39.97-68.97 wt.% ThO_2 in the altered granite, so they are similar but have a higher variability in the altered granite (Table 3). The same observation can be made for the SiO_2 wt.% contents, ranging between 7.37-17.69 in thorite from unaltered granite and between 8.18-18.07 in altered granite. The analytical totals are low either in thorite from the unaltered granite (75.49 - 91.26 wt.%) or the altered granite (75,71- 96.54 wt.%), which can be due to some hydratation.

The U, Y, P, REE, Fe, Ca, Pb, and F contents of thorite from the altered granite are similar to those of thorite from the unaltered granite (Table 2). The UO_2 wt.% concentrations in thorite range between 0.45 to 8.63 in the unaltered granite and between 0.46 to 10.43 in the altered granite. The Y_2O_3 wt.% concentrations range from 0.01 to 5.62 in the unaltered granite and from 0.07 to 4.20 in the altered granite.

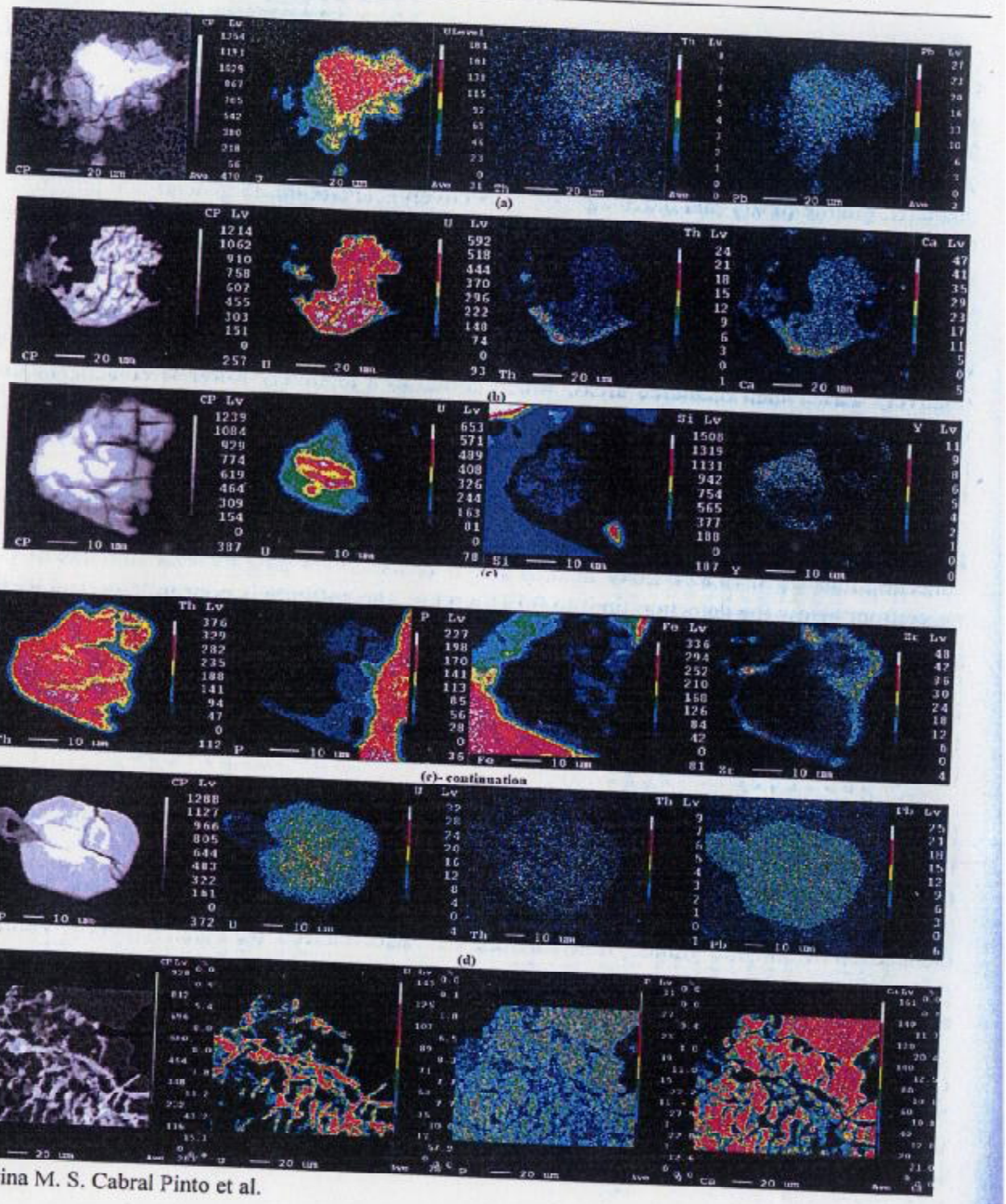

Marina M. S. Cabral Pinto et al.

Figure 3. X-ray elements maps, obtained by the electron-microprobe, of minerals from the altered granite and hydrothermal quartz veins. (a) – Altered crystal of uraninite from the altered granite. (b)– Altered crystal of coffinite from the altered granite. (c) – Altered crystal of thorite from the altered granite. (d) – Altered crystal of xenotime from the altered granite. (e) – Crystal of apatite replaced by (meta)saleeite from hydrothermal quartz veins.

In the altered granite, thorite occurs filling fractures of other minerals, such as apatite, monazite and biotite (Figure 2s-x), mainly in their rims (Figure 2e, g, r, v) and seems to replace monazite along fractures, associated with xenotime (Figure 2q). A zoned crystal of thorite was analysed (crystal B in Table 2) in the altered granite and the darker rim is poorer in Si, U, Y, Ca, ΣREE and richer in P, Th, Fe, Pb, F than the respective lighter core (Figure 2e, Table 2).

Figure 3c presents a X-ray map of a fractured thorite grain from the most altered granite (crystal A, Table 2) and close to the fractures the crystals are more altered and darker than in the areas away from those fractures, which may be due to the decrease of U contents. The most altered areas close to the fractures are clearly poorer in U and Si (0.46-3.87 wt.% UO_2 and 9.95-12.99 wt.% SiO_2), than areas away from the fractures (7.23-10.43 wt.% UO_2 and 16.03-16.45 wt.% SiO_2) (Table 2 and Figure 3c). These most altered areas are richer in P, Fe, Pb, F and Zr than the unaltered areas (Table 2). So the altered thorite is the poorest in U and Si and the richest in P, Fe, Pb and F in its rims and close to the fractures. The distribution of Zr is not homogeneous in the most altered areas (like that of Pb), but Zr seems to surround thorite crystal (Figure 3c).

Chemical compositions of zircon from the unaltered granite and mineralized quartz veins were presented by CABRAL PINTO et al. (2008). Zircon compositions from the altered granite and new analyses of zircon from the mineralized quartz veins are given in Table 3. In general, zircon from the unaltered granite has the lowest mean Fe, P, U and Pb contents (0.20 wt.% Fe_2O_3, 0.12 wt.% P_2O_5, 0.05 wt.% UO_2, 0.07 wt.% PbO) and the highest mean Zr and Hf content (65.24 wt.% ZrO_2, 1.42 wt.% HfO, Table 3 and CABRAL PINTO et al, 2008). In general, zircon from altered granite has the highest mean of P (0.40 wt.% P_2O_5), Y (0.55 wt.% Y_2O_3), U (0.22 wt.% UO_2), La+Ce (0.28 wt.% REE_2O_3), Pb (0.23 wt.% PbO) and the lowest mean of analytical totals, Si and Zr (30.56 wt.% SiO_2, 61.29 wt.% ZrO_2), whereas the mean Hf concentrations is similar to that in zircon from mineralized quartz veins (Table 3). In the unaltered granite, zircon does not present significant chemical variation either within grains or between grains, but the distribution of U in the altered grains shows a chemical zonation, and the rim contains more U (up to 0.62 wt.% UO_2) than the core (Table 3). However some altered crystals present an inverse zonation, with loss in U in the rims (Table 3). Zircon from mineralized quartz veins has the highest mean contents of Mg (0.14 wt.% MgO) and 0.13 wt.% UO_2, but very high values of U (~15 wt.%, UO_2) were found in the rims of some dissolved and altered crystals (Table 3). These rims with high U contents have very low contents of SiO_2 (~18 wt.%), ZrO_2 (~43 wt. %), analytical totals (~89 wt.%) and very high values of P_2O_5 (~3 wt.%) and Fe_2O_3 (1.3 wt.%) (Table 3). Therefore, numbers of cations per chemical formula were not calculated. The composition of the respective unalterated cores is close to $[(Zr,Hf)SiO_4]$ and U contents are similar to those found in the zircon from altered granite (Table 3). CABRAL PINTO et al. (2008) also presented values of UO_2 (~18 wt.%), Fe_2O_3 (~8 wt.%), SiO_2 (~14 wt.%) and ZrO_2 (41 wt.%) in the rims of very altered zircon crystals.

The chemical analyses of xenotime (YPO_4) are presented in Table 3. There is no significant difference between the chemical composition of xenotime from the unaltered and altered granites, except for the U content which is lower (mean of 1.57 wt.% UO_2) in the xenotime from the altered granite, whereas it has a mean of 2.35 wt.% UO_2 in xenotime from the unaltered granite (Table 3). The rims of xenotime crystals from the altered granite are poorer in U than respective cores (Table 3 and Figure 3d).

Table 3. Chemical composition (in weigh percent) and structural formula of zircon and xenotime from the Variscan unaltered and altered granites and associated hydrothermal quartz veins, Central Portugal

	Zircon												Xenotime											
	Unaltered granite		Altered granite						Mineralized quartz vein				Unaltered granite		Altered granite							Quartz veins	
											Grain cores	Grain rims			Profile of a crystal								
	Mean	σ	Mean	σ	core	rim	core	rim	Mean	σ			Mean	σ	Mean	σ	rim	rim	core	core	rim	rim	Mean	σ
SiO_2	31.50	0.89	30.56	1.14	31.48	28.03	28.03	30.89	34.16	3.78	35.14	35.48	17.86	18.31	P_2O_5	Mean	σ	Mean	σ	rim	rim	core	core	rim	rim	Mean	σ
ZrO_2	63.25	2.78	61.29	3.21	66.11	58.01	61.03	61.67	61.74	3.54	62.68	62.20	43.00	42.86	SiO_2	33.66	0.38	34.02	0.38	33.89	34.10	34.22	33.31	33.87	32.92	32.86	0.75
HfO_2	1.42	0.23	1.31	0.37	1.58	1.43	0.01	1.42	1.51	0.21	1.36	1.10	1.12	1.44	TiO_2	0.70	0.20	0.71	0.16	0.68	0.61	0.63	0.35	0.66	0.60	n.d.	n.d.
ThO_2	0.01	0.02	0.03	0.02	0.02	—	—	—	0.05	0.07	0.02	-	0.41	0.43	ZrO_2	—	—	—	—	—	—	—	—	—	—	n.d.	n.d.
Al_2O_3	0.16	0.12	0.34	0.43	0.03	—	0.20	0.08	0.21	0.27	0.19	0.09	2.45	2.31	HfO	—	—	—	—	—	—	—	—	—	—	0.70	0.16
Fe_2O_3	0.20	0.16	0.36	0.19	0.18	0.66	0.34	0.27	0.21	0.20	0.33	0.30	1.24	1.27	ThO_2	0.21	0.02	0.28	0.02	0.22	0.27	0.27	0.28	0.25	0.22	—	—
MgO	0.01	0.07	0.07	0.13	0.02	—	0.01	0.01	0.04	0.04	0.22	0.18	0.85	0.55	UO_2	0.16	0.10	0.18	0.03	—	0.13	0.12	0.26	0.17	—	0.44	0.21
MnO	0.01	0.04	0.04	0.03	n.d.	n.d.	—	0.02	0.04	0.03	—	0.04	0.08	0.16	Y_2O_3	2.35	0.49	1.57	0.38	1.62	1.28	1.84	2.10	1.38	1.62	0.45	0.37
WO_3	0.05	0.10	0.11	0.10	n.d.	n.d.	—	—	0.07	0.05	—	—	0.36	0.33	La_2O_3	38.50	0.28	39.25	0.83	39.13	40.51	38.71	36.77	38.20	36.14	43.46	1.01
K_2O	0.01	0.02	0.02	0.02	n.d.	n.d	0.01	—	0.13	0.17	—	—	—	—	Ce_2O_3	—	—	-	—	—	—	—	—	—	—	—	—
Y_2O_3	0.15	0.25	0.56	0.39	0.03	0.06	n.d.	n.d.	0.32	0.42	0.03	—	1.81	1.70	Pr_2O_3	0.06	0.09	0.03	0.03	0.04	0.06	0.01	0.05	0.09	0.01	0.04	0.02
La_2O_3	0.10	0.09	0.14	0.06	n.d.	n.d.	0.25	—	0.04	0.03	—	—	0.02	—	Nd_2O_3	0.01	0.01	0.01	0.01	—	0.03	0.01	—	—	—	0.05	0.07
Ce_2O_3	0.07	0.13	0.14	0.14	n.d.	n.d.	—	0.02	0.05	0.03	0.05	0.05	0.19	0.29	Sm_2O_3	0.37	0.06	0.35	0.04	0.28	0.34	0.37	0.35	0.40	0.37	0.12	0.03
CaO	0.07	0.24	0.36	0.51	—	—	0.54	0.45	0.08	0.13	2.07	0.02	0.61	0.73	Eu_2O_3	0.03	0.06	0.04	0.11	0.01	0.07	0.03	0.06	0.04	0.01	0.03	0.03
PbO	0.07	0.11	0.23	0.16	—	0.06	0.25	0.53	0.15	0.11	0.05	—	0.02	0.13	Gd_2O_3	n.d.	n.d.	n.d.	n.d.	n.d.	n.d.	n.d.	n.d.	n.d.	n.d.	0.28	0.10
UO_2	0.05	0.11	0.22	0.15	—	0.07	0.02	0.24	0.13	0.21	3.89	0.18	15.07	13.87	Tb_2O_3	1.91	0.15	1.60	0.35	2.57	1.90	1.81	1.77	1.88	2.06	3.27	0.68
ThO_2	0.05	0.10	0.03	0.09	0.05	—	0.14	0.06	0.06	0.06	0.03	0.09	0.73	0.59	Dy_2O_3	n.d.	n.d.	n.d.	n.d.	n.d.	n.d.	n.d.	n.d.	n.d.	n.d.	0.45	0.07
P_2O_5	0.82	0.31	0.49	0.21	0.21	0.82	n.d.	n.d.	0.17	0.17	0.18	—	3.08	3.13	Ho_2O_3	0.47	0.06	0.51	0.55	0.54	0.70	0.28	0.12	0.28	0.34	0.54	0.13
Total	99.16	2.89	96.17	3.31	98.68	87.54	92.73	95.68	98.19	2.36	101.52	98.84	85.15	88.15	Er_2O_3	1.67	0.08	1.11	0.04	1.18	1.08	1.08	1.12	1.16	1.16	2.74	0.22
															Tm_2O_3	2.34	0.26	2.22	0.43	1.77	3.09	2.41	2.62	2.57	1.78	3.81	0.17
Si	1.037	0.012	1.022	0.038	1.034	1.000	1.000	1.007	1.136	0.110	1.156	1.201			Yb_2O_3	n.d.	n.d.	n.d.	n.d.	n.d.	n.d.	n.d.	n.d.	n.d.	n.d.	0.60	0.06
P	0.023	0.014	0.023	0.022	0.009	0.027	—	—	—	—	—	—			Lu_2O_3	5.14	0.26	5.10	0.44	3.46	3.80	3.20	3.33	3.27	2.45	2.71	0.29
Al^{IV}	0.006	0.012	0.017	0.038	0.004	—	0.001	0.013	0.035	0.038	0.026	0.012			FeO	0.67	0.03	0.64	0.05	0.66	0.72	0.68	0.58	0.62	0.56	0.82	0.08
Σ	3.915	0.053	4.01	0.05	3.96	4.01	3.97	4.00	4.220	0.112	4.224	4.273			CaO	0.13	0.04	0.11	0.07	0.22	0.07	0.11	0.05	0.02	0.22	n.d.	n.d.
Al^{VI}	—	0.028	—	0.057	—	—	—	0.038	—	—	—	—			PbO	0.08	0.06	0.04	0.05	0.28	0.13	0.27	0.21	0.23	0.28	n.d.	n.d.
Zr	3.966	0.074	3.835	0.085	3.964	3.838	3.862	3.881	3.890	0.108	3.857	3.845			F	0.15	0.06	0.15	0.07	0.07	0.10	0.24	0.15	0.08	0.06	n.d.	n.d.
Hf	0.051	0.008	0.048	0.011	0.050	0.052	—	0.052	0.040	0.010	0.048	0.038			Total	0.02	0.02	0.03	0.04	—	0.01	—	0.02	0.06	—	n.d.	n.d.
Fe^{3+}	0.019	0.017	0.029	0.020	0.015	0.075	0.024	0.035	0.028	0.008	0.033	0.037				92.36	0.85	92.23	0.80	91.67	95.24	92.05	91.54	91.00	91.50	99.48	0.56
Mg	0.004	0.013	0.013	0.024	0.004	—	0.002	0.002	0.008	0.012	0.038	0.028			P												
Ti	0.001	0.002	0.003	0.002	0.002	—	—	—	0.001	0.001	0.001	—			Si	4.031	0.044	4.041	0.03	1.040	1.016	1.046	1.006	1.048	1.001	3.946	0.041
Pb	0.002	0.004	0.003	0.008	—	0.003	0.006	0.018	0.006	0.008	0.002	—			Ti	0.111	0.027	0.100	0.02	0.096	0.126	0.088	0.135	0.083	0.087	n.d.	n.d.
U	0.001	0.003	0.004	0.005	—	0.010	0.006	0.007	0.004	0.006	0.024	0.006			Zr	—	—	—	—	—	—	—	—	—	—	n.d.	n.d.
Th	0.001	0.002	0.002	0.003	0.001	—	0.004	0.002	0.002	0.002	0.002	0.002			Hf	—	—	—	—	—	—	—	—	—	—	0.004	0.010
Y	0.008	0.011	0.035	0.020	0.002	0.004	n.d	n.d	0.009	0.017	0.003	—			Th	0.011	0.001	0.012	0.001	0.010	0.012	0.012	0.013	0.015	0.010	—	—
La	0.001	0.001	0.005	0.003	n.d.	n.d.	0.009	—	0.002	0.001	—	—			U	0.005	0.003	0.001	0.003	—	0.004	0.004	0.009	0.004	—	0.011	0.007
Ce	0.005	0.003	0.003	0.003	n.d.	n.d.	—	—	0.001	0.001	0.001	0.001			Y	0.074	0.019	0.049	0.012	0.032	0.042	0.037	0.066	0.043	0.032	0.011	0.011
Dy	0.009	0.005	0.049	0.015	—	—	0.007	0.002	0.007	0.015	0.009	0.002			La	2.920	0.020	2.955	0.027	2.939	2.972	2.951	2.930	2.938	2.958	3.200	0.059
Σ	4.07	0.05	4.04	0.07	4.04	3.98	4.10	4.06	3.950	0.118	3.814	3.752			Ce	—	—	—	—	-	-	-	-	-	-	-	-
N	n=71		n=20						n=56						Pr	0.003	0.001	0.002	0.002	- -	0.003	0.001	0.001	0.005	—	0.002	0.002
															Nd	—	—	—	0.001	—	0.002	—	—	—	—	0.008	0.004
															Sm	0.018	0.002	0.015	0.002	0.018	0.017	0.020	0.015	0.020	0.018	0.006	0.001
															Eu	0.030	0.003	0.031	0.01	0.029	0.032	0.029	0.027	0.031	0.029	0.026	0.005
															Gd	n.d.	n.d.	n.d.	n.d.	n.d.	n.d.	n.d.	n.d.	n.d.	n.d.	0.014	0.005
															Tb	0.089	0.008	0.093	0.017	0.130	0.079	0.084	0.093	0.088	0.120	0.150	0.028
															Dy	n.d.	n.d.	n.d.	n.d.	n.d.	n.d.	n.d.	n.d.	n.d.	n.d.	0.098	0.005

—: not detected. n.d.: not determined. Cation formula based on sixteen atoms of oxygen for zircon and xenotieme. n: number of analysis.

Table 4 . Chemical composition (in weigh percent) and structural formula of monazite and apatite from the Variscan unaltered and altered granites and associated hydrothermal quartz veins, and U-phosphates from the hydrothermal quartz veins, Central Portugal

	Monazite								Apatite									U-phosphates								
	Granite					Quartz veins			Granite					Quartz veins				Mineralized quartz veins								
	Unaltered granite			Altered granite		Quartz veins			Unaltered granite		Altered granite							Associated with apatite								
																		Meta-saleeite		Autunite			Meta-autunite		Saleeite	
	Mean	σ	Crystal	Mean	σ	Mean	σ		Mean	σ	Mean	σ	Rec. crystal	Mean	σ	Crystal A		Mean	σ	Mean	σ	Crystal	Mean	σ	Mean	σ
P_2O_5	28.44	0.79	29.89	30.08	0.84	30.54	0.44	P₂O₅	41.17	0.46	38.87	2.89	39.09	41.38	1.34	39.47	P₂O₅	39.72	0.33	39.77	0.75	41.83	39.82	0.53	39.95	0.73
SiO_2	0.20	0.10	0.31	0.37	0.32	0.44	0.50	SiO₂	1.56	1.00	1.54	—	—	—	—	—	SiO₂	0.01	0.01	—	—	—	—	—	0.34	0.00
Gd_2O_3	26.38	1.47	25.80	26.34	1.31	29.99	1.13	CaO	52.65	1.13	49.21	2.07	49.29	53.18	0.59	53.93	MgO	4.27	0.24	4.32	0.20	4.14	4.22	0.23	4.18	0.32
La_2O_3	10.45	1.05	9.52	11.08	0.95	13.47	1.82	SrO	0.03	0.03	0.04	0.02	0.06	n.d.	n.d.	n.d.	TiO_2	0.03	0.03	0.05	0.05	—	0.05	0.04	0.03	0.02
Nd_2O_3	10.84	0.58	10.47	10.45	0.85	13.21	1.53	Na_2O	0.11	0.04	0.05	0.04	0.15	0.01	—	0.01	CaO	0.69	0.28	0.69	0.24	0.51	0.07	0.05	0.13	0.00
Pr_2O_3	2.57	0.51	2.70	2.63	0.20	2.64	0.77	K_2O	0.04	0.04	0.01	0.03	0.08	—	—	—	ZnO	n.d.	n.d.	n.d.	n.d.	n.d.	0.18	0.30	0.23	0.03
Sm_2O_3	1.84	1.18	2.78	—	—	1.55	1.07	P_2O_5	41.17	0.46	38.87	2.89	39.09	41.38	1.34	39.47	Y_2O_3	n.d.	n.d.	n.d.	n.d.	n.d.	0.01	0.01	0.02	0.04
Gd_2O_3	0.80	0.33	n.d.	3.04	0.39	n.d.	n.d.	SiO_2	0.16	0.20	1.56	1.00	1.54	—	—	—	PbO	0.05	0.05	0.01	0.01	—	0.10	0.13	0.00	0.00
Dy_2O_3	0.91	0.21	n.d.	0.67	0.14	n.d.	n.d.	ThO_2	—	0.01	0.02	0.03	0.06	0.01	0.02	n.c.	ThO_2	0.01	0.01	0.01	0.01	—	—	0.01	0.01	0.05
Ho_2O_3	—	—	n.d.	—	—	n.d.	n.d.	Al_2O_3	0.05	0.06	0.56	0.28	0.67	0.04	0.01	0.04	UO_2	58.38	9.04	58.74	2.59	40.34	61.45	0.87	59.84	1.24
Er_2O_3	—	—	n.d.	—	0.01	n.d.	n.d.	BaO	—	—	—	—	—	n.d.	n.d.	n.c.	La_2O_3	0.01	0.01	0.01	0.01	—	0.02	0.04	—	—
Yb_2O_3	—	0.01	n.d.	—	—	n.d.	n.d.	PbO	0.01	0.03	—	—	—	—	—	0.01	Ce_2O_3	0.03	0.04	—	—	—	0.02	0.03	0.03	0.03
La_2O_3	0.07	0.05	n.d.	0.25	0.07	n.d.	n.d.	UO_2	0.01	0.01	—	0.01	0.01	0.18	0.08	1.03	Na_2O	n.d.	n.d.	n.d.	n.d.	n.d.	0.06	0.17	0.04	0.04
Pr_2O_3	0.07	0.12	—	0.08	0.15	0.48	1.08	ThO_2	0.01	0.01	0.55	0.48	0.65	—	—	—	K_2O	n.d.	n.d.	n.d.	n.d.	n.d.	0.06	0.07	0.01	0.02
CaO	1.73	0.18	2.18	1.42	1.31	0.24	0.17	Y_2O_3	0.28	0.07	0.47	0.25	0.35	—	—	—	SiO_2	0.26	0.06	0.01	0.02	0.02	0.47	0.37	0.23	0.28
PbO	0.18	0.13	0.04	0.17	0.08	0.03	0.07	La_2O_3	0.04	0.08	0.01	0.28	0.24	—	—	3.02	Al_2O_3	0.15	0.07	0.24	0.14	0.08	0.04	0.03	0.10	0.10
Al_2O_3	0.05	0.11	—	0.14	0.19	0.13	0.32	Ce_2O_3	0.11	0.08	0.52	0.30	0.30	—	—	3.02	P_2O_5	16.81	0.86	15.53	0.51	15.31	15.82	0.23	15.14	0.43
Y_2O_3	2.14	0.75	2.01	2.38	0.62	0.57	0.23	F	2.24	3.90	2.09	0.47	2.93	2.70	0.15	2.82	F	0.45	0.54	0.48	0.09	0.30	n.d.	n.d.	0.0	0.0
ThO_2	7.91	1.01	8.80	8.64	0.78	4.14	0.98	Cl	0.02	0.02	0.01	0.01	—	0.01	0.01	0.01	Total	83.79	1.01	80.55	0.60	82.30	83.42	0.94	81.07	1.65
UO_2	1.36	0.53	2.04	0.77	0.48	0.19	0.10	Total	97.67	1.97	93.42	2.75	99.27	98.00	1.43	97.01										
ZrO_2	0.01	0.01	n.d.	0.02	0.02	n.d.	n.d.	O≡F	0.95		0.88		0.99	1.10		1.15	Fe	0.004	0.040	0.007	0.006	0.213	0.000	0.002	0.124	0.030
HfO	0.02	0.01	n.d	0.01	0.01	n.d.	n.d.	O≡Cl	—		—		—	—		n.d.	Mn	0.001	0.001	—	—	—	—	—	0.000	0.000
MgO	n.d.	n.d.	n.d.	n.d.	n.d.	0.01	0.02	Total	96.72		92.54		98.28	96.90		95.91	Mg	0.885	0.071	0.879	0.054	0.871	0.901	0.071	0.887	0.080
F	0.27	0.17	0.39	0.20	0.13	0.49	0.19										Ti	0.003	0.004	0.005	0.003	—	0.005	0.004	0.004	0.002
Total	97.58	1.76	96.20	96.62	3.42	83.11	2.11										Ca	0.102	0.030	0.130	0.043	0.088	0.010	0.008	0.021	0.010
O≡F	0.10	0.07	0.16	0.08	0.05	0.18		P	5.000	0.053	5.025	0.212		5.058	0.031	5.028	Zn	n.d.	n.d.	n.d.	n.c.	n.d.	0.008	0.020	0.054	0.026
Total	97.68	1.76	96.04	96.54	3.43	82.93		Si	0.021	0.034	0.282	0.184		...	—	—	V	n.d.	n.d.	n.d.	n.d.	n.d.	0.001	0.001	0.002	0.002
								Σ	5.01	0.08	5.01			5.06	0.03	5.03	Pb	0.002	0.002	—	—	—	0.004	0.005	0.001	0.001
P	3.882	0.037	3.994	4.052	0.040	4.028	0.100	Al	0.009	0.017	0.923	0.081		0.009	0.011	0.007	Th	—	—	—	—	—	—	—	0.001	0.002
Si	0.032	0.021	0.017	0.038	0.053	0.008	0.001	Mg	0.005	0.005	0.055	0.050		0.022	0.011	0.048	U	1.508	0.181	1.055	0.123	2.102	1.051	0.081	2.480	0.056
P+Si	3.88		4.01	4.07		4.10		Fe	0.072	0.045	0.089	0.070		0.008	0.005	0.009	La	—	—	—	—	—	0.002	0.002	—	—
Ca	1.490	0.008	1.384	1.462	0.072	1.031	0.006	Mn	0.078	0.021	0.012	0.010		0.004	0.004	n.d.	Ce	0.001	0.002	—	—	—	0.001	0.001	0.003	0.002
La	0.011	0.009	0.008	0.045	0.006	0.028	0.015	Na	0.007	0.012	0.018	0.016		0.003	0.001	0.003	Na	n.d.	n.d.	n.d.	n.d.	n.d.	0.022	0.007	0.012	0.010
Nd	0.014	0.002	0.004	0.011	0.005	0.007	0.004	K	0.005	0.008	0.040	0.029		—	—	—	X	n.d.	n.d.	n.d.	n.d.	n.d.	0.010	0.014	0.002	0.004
Pr	0.148	0.010	0.158	0.151	0.008	0.160	0.047	Ca	9.453	0.182	8.525	0.451		9.538	0.193	8.885	Si	0.008	0.011	0.001	0.003	2.988	0.063	0.060	0.038	0.030
Sm	0.002	0.005	0.102	—	—	0.005	0.001	Sr	—	—	—	—		n.d.	n.d.	n.d.	Al	0.028	0.011	0.043	0.023	3.018	0.007	0.008	0.024	0.018
Gd	0.030	0.005	n.d.	0.109	0.013	n.d.	n.d.	Ba	—	—	—	—		n.d.	n.d.	n.d.	P	1.002	0.011	1.008	0.003	2.000	0.992	0.008	2.000	0.030
Dy	0.046	0.021	n.d.	0.034	0.006	n.d.	n.d.	Pb	0.001	0.001	—	—		—	—	—										
Ho	—	—	n.d.	—	—	n.d.	n.d.	U	—	—	—	—		0.003	0.010	0.042	H_2O	3		10		10	5		10	
Er	—	—	n.d.	—	—	n.d.	n.d.	Th	—	—	0.023	0.029		—	—	—	F+Si	2.00		2.00		2.00	2.00		2.00	
Yb	—	—	n.d.	—	—	n.d.	n.d.	Σ	9.57	0.23	9.90	0.50		9.63	0.23	10.10	Σ	1.97		1.21		1.27	1.01		1.12	
La	0.003	0.002	n.d.	0.002	0.001	n.d.	n.d.										U	1.87		1.98		2.10	1.95		2.05	
Fe	0.008	0.004	—	0.008	0.018	0.008	0.135	F	1.158	0.157	1.187	0.262		1.457	0.138	1.432		n=10		n=8			n=12		n=12	
Ca	0.284	0.001	1.388	0.240	0.048	0.049	1.010	Cl	0.007	0.008	0.008	0.004		0.002	0.002	0.002										
Pb	0.004	0.008	0.009	0.007	0.000	0.001	1.033	Oh	0.785	0.158	0.810	0.280		0.541	0.072	0.566										
Al	0.010	0.020	—	0.028	0.039	0.028	0.011		n=27		n=14			n=16												

—: not detected. n.d.: not determined. Cation formula based on sixteen atoms of oxygen for monazite, twenty five atoms of oxygen for apatite. Cation formula based on two atoms of P (+ Si) for saleeite and meta-saleeite, Σ=Fe+Mn+Mg+Ca+Y+Na+K. n: number of analysis.

Xenotime from mineralized quartz veins is poorer in P, U, Nd, and richer in Y, Th, Gd, Dy, Ho, Er, Lu than xenotime from the unaltered and altered granites (Table 3). The xenotime from mineralized quartz veins has a mean content of 0.45 wt.% UO_2 and 43.49 wt.% Y_2O_3, whereas xenotime from unaltered and altered granite have mean concentrations of 1.57-2.35 wt.% UO_2 and 38.90-39.29 wt.% Y_2O_3, but a value of 1.02 wt.% UO_2 occurs in the rims of altered crystals (Table 3). The HREE are 0.690-0.692 a.p.f.u. in xenotime from the unaltered and altered granites and 0.980 a.p.f.u. in xenotime from mineralized quartz veins. The LREE are low and of 0.050-0.053 a.p.f.u. in xenotime from unaltered and altered granites and 0.035 a.p.f.u. in xenotime from quartz veins (Table 3). Hafnium, Fe, Ca and Pb were detected in xenotime from the granites but were not found in xenotime from mineralized quartz veins (Table 3). Thorium contents are similar in xenotime from all granite samples, but slightly higher Th contents were found in xenotime from quartz veins (Table 3).

The chemical composition of Ce-monazite from the unaltered granite was presented by CABRAL PINTO et al. (2008), but more new analyses are given in Table 4. Chemical composition of monazite in the altered granite is more variable than in the unaltered granite and has generally higher mean contents of Si, Al and lower mean contents of U (0.77 wt.% U_3O_8), Ca, Th (6.84 wt.% ThO_2) and F (0.20 wt.% F) than Ce-monazite from the unaltered granite (up to 2.04 wt.% U_3O_8, 0.27 wt.% F, and 9.60 wt.% ThO_2, Table 4).

The Ce-monazite from the mineralized quartz veins is the poorest in Ca, Y, Th, U and the richest in Si, Fe, LREE and F (Table 4). It has mean concentrations of 0.19 wt.% U_3O_8 and 1.14 wt.% ThO_2 and a low analytical total (Table 4).

Chemical analyses of apatite from the granite and related hydrothermal quartz veins are given in Table 4. They are F-apatites. In the altered granite and in mineralized quartz veins, the apatite grains are vacuolated and show a high porosity (Figure 3e and Figure 2c, s-w, ac) indicating apatite dissolution. Apatite from the altered granite generally has higher mean contents of Fe, Mg, K, Si, Al, Th, Y, La, Ce, and lower mean contents of Mn, Ca, Na, P, U, F, and analytical totals, than apatite from the unaltered granite, but the analytical variability is high in apatite from the altered granite (Table 4). The most fractured apatite grain from the altered granite has a low analytical total (85.29 wt.%) and P concentration (30.09 wt.% P_2O_5) so its structural chemical formula was not calculated (Table 4). Uranium contents are always low in apatite from the unaltered and altered granites, but they reach 1.09 wt.% UO_2 in apatite from mineralized quartz veins (Table 4). Apatite from hydrothermal quartz veins has mean contents of Ca and P similar to the apatite from the unaltered granite, but higher mean contents of U and F (0.13 wt.% UO_2, and 2.76 wt.% F) and Y, La and Ce were not detected in this apatite (Table 4). Apatite crystals from the mineralized quartz veins associated with uranium-phosphate phases have the highest U (1.09 wt.% UO_2) content (crystal A in Table 4 and Figure 3e). This apatite is richer in Fe and poorer in P than the apatite not associated with uranium-phosphate phases (Table 4, crystal A).

The chemical composition of saleeite, meta-saleeite, ferrous-substituted-saleeite, $(Mg, Fe^{2+})(UO_2)_2(PO_4)_2{\cdot}4H_2O$ and other U-phosphate phases with similar compositions but with different H_2O contents, from mineralized quartz veins, were presented by CABRAL PINTO and SILVA (2007) and CABRAL PINTO et al. (2008). Now, more saleeite and meta-saleeite analyses from the hydrothermal quartz veins are presented in Table 4. Some U-phosphates are associated with apatite (Figure 2ad and Figure 3e), while others are not (Figure 2af).

In general, uranium phosphates associated with apatite have lower FeO and higher MgO and CaO than those not associated with apatite. However crystals with high Fe contents were also found in (meta)saleeite associated with apatite (Table 4).

DISCUSSION

Uraninite is the main host of uranium in the unaltered peraluminous biotite granite, which has A/CNK ranging from 1.08 to 1.16 (SILVA AND NEIVA 1999/2000). In peraluminous granites, uraninite is the host of considerable bulk-rock uranium content (FÖRSTER 1999) and is the most important uranium mineral in terms of abundance, occurrence and economic value (FINCH AND MURAKAMI 1999). The disposal of UO_2 from used nuclear fuel is an environmental issue; so the studies of stability, alteration and leaching of uraninite are numerous (GRANDSTAFF 1976, LANGMUIR, 1978, PARKS AND POHL 1988, FINCH AND EWING 1992, JANECZEK AND EWING 1992A,B, PEARCY et al. 1994, FAYEK et al. 1997, JENSEN et al. 1997, FINCH AND MURAKAMI 1999, JENSEN AND EWING 2001, JERDEN AND SINHA 2003, EVINS et al. 2005, BRUNO AND EWING 2006, DEDITIUS et al. 2007).

Under oxidizing conditions uraninite gives rise to many complex uranyl minerals, such as carbonates (e.g. bijvoetite, urancalcarite, znucalite, etc.), silicates (e.g.: coffinite, sklodowskite, soddyite, swamboite), phosphates (e.g. yingjiangite, autunite and meta-autunite, saleeite, metasaleeite, etc.), oxyhydroxides (e.g.: clarkeite, ianthinite, vandendriesscheite, etc.), vanadates (e.g. carnotite, curiénite, etc.), molybdates (e.g. calcurmolite, cousinite, etc.), arsenates etc. (KOTZER AND KYSER 1993, GAINS ET AL. 1997, FINCH AND MURAKAMI 1999).

Uraninite occurs mainly in the unaltered granite and is magmatic (CABRAL PINTO et al. 2008); it is rare in the altered granite and was not found in mineralized quartz veins. In the unaltered granite, some uraninite crystals are zoned with rims enriched in U and poorer in Th than cores (Table 1 and CABRAL PINTO et al, 2008), which reflect the Th-U substitutions. The uraninite from the unaltered granite is richer in U, Pb, Ca, Fe and poorer in Si and F than the uraninite from the altered granite (Table 1). In the altered granite, uraninite shows fractures and vacuoles and has the radioactive damage halos filled with late pyrite, U-S-bearing phases and Fe oxyhydroxides (Figure 2 j-k). The analytical totals of uraninite are lower in the altered granite than in the unaltered granite (Table 1). Crystal rims of uraninite from the altered granite are poorer in U than the respective core and rims and cores of zoned uraninite crystals from the unaltered granite (Table 1 and Figure 3a). Locally, in the altered granite, uraninite is replaced by coffinite, but the U contents of this uraninite are similar to that of the altered uraninite (Table 1, analyses 1, 2). In general, the hydrothermal alteration caused a decrease in U, Pb, Ca, Fe and an increase in Si and F in the uraninite (Table 1) indicating uranium removal from crystal rims and alteration zones and the formation of coffinite.

Coffinite $U[SiO_4]_{1-x}(OH)_{4x}$ (Gaines et al., 1997), is a tetragonal orthosilicate with zircon-type structure. The U-Th silicates, thorite and coffinite are usually metamitic and can incorporate molecular H_2O, and the formula $(U,Th)SiO_4.nH_2O$ (n<4) used by various authors (e.g. SPEER 1982, LUMPKIN AND CHAKOUMAKOS 1988, SMITHS 1989, JANECZEK 1991, FINCH AND MURAKAMI 1999) is equally valid (GAINES et al. 1997). According to FINCH AND MURAKAMI (1999), the U-Th silicates form two series of anhydrous and hydrated minerals

with the chemical formulas: $(U,Th)SiO_4$ and $(U,Th)SiO_4.nH_2O$ ($n<4$). The hydrated U(IV)-silicate, coffinite, was only found in the most altered granite and some crystals replace uraninite (Figure 2l). So, coffinite results from uraninite alteration, since uraninite is unstable in supergenic and hydrothermal environments (POTY et al. 1986, GAINES et al. 1997). The lower analytical totals found in the analysed coffinite (Table 1) are probably due to the presence of OH or H_2O as there are coffinite analyses close to 100% and all the analyses were performed with the same analytical procedures. The analysed coffinite is close to the end member ($USiO_4$). Coffinite crystals are altered and a compositional heterogeneity core-rim was observed, with an impoverishment in U in the crystal rims, with lower UO_2 contents up to 10 wt.%, relatively to the respective cores, and enrichment in Th and Ca in the crystal rims (Table 1 and Figure 3b). The low U contents (0.924 and 0.886 a.p.f.u.) found in the crystals rims are due to alteration and indicate uranium mobilization from coffinite.

Thorite is widespread in the unaltered and altered granites. Thorite seems to be magmatic in the unaltered granite (Figure 2b), but secondary thorite was found in the altered granite and related to the chloritization of biotite (Figure 2e,o, w) and alteration of apatite (Figure 2c) and plagioclase (Figure 2p). Locally it is zoned (Figure 3c and Table 2) and occurs associated with zircon, but the textural relation does not allow to find out if it is a product of zircon alteration (Figure 2p), as found by RUBIN et al. (1989). In the altered granite, thorite replaces apatite (Figure 2c, g, v) and monazite (Figure 2f, q, t), is associated with xenotime, and fills fractures of biotite.

Thorite composition is quite variable (Table 2), which agrees with SPEER (1982) and FORSTER (2006). The analytical totals are low, ranging from 75.71 to 96.54, but the analyses are close to stoichiometry (totals of 2.07 to 2.27 a.p.f.u, Table 2). These low totals are probably attributed to hydratation, because thorite is highly metamitic, and the WDS scan did not show the presence of other elements. The high contents of Fe, Ca, Zr and P can indicate some analytical interferences (FORSTER 2006), because thorite occurs as very small crystals associated with zircon, xenotime and replaces monazite and apatite (Table 2, Figure 2c, e-g, p-w), whereas the high contents of Y and Zr may suggest a solid solution with xenotime and zircon (FORSTER 2006). Thorite forms a solid solution with coffinite (FORSTER 2006), but the analysed coffinite is almost pure $USiO_4$. The U contents in thorite range from 0.45 to 10.43 UO_2 wt.% UO_2 (Table 2 and Figure 4a).

The U, Y, P, REE, Fe, Ca, Pb, and F contents are not significantly different in thorite from the unaltered and altered granites, so it seems that there is no significant difference in the chemical composition of thorite from these granites. However, in thorite from the unaltered granite there are a regular decrease in U content with increasing P (Figure 4b) content and an enrichment of (Y+HREE) relatively to LREE (Figure 4c) as found by HETHERINGTON AND HARLOV (2008), but they were not found in thorite from the altered granite. So there are two generations of thorite, the first is primary and belongs to the unaltered granite and the second results from alteration of other minerals like monazite and apatite. In the altered granite, the zoned crystals of thorite have rims poorer in U, Si, Y, Ca, REE and richer in P, Th, Fe, Pb and F than the respective cores; also in the altered zones close to the fractures, thorite is poorer in U, Si and richer in P, Fe, Pb and F than in unaltered zones (Table 2 and Figure 3c). So U and Si are mobilized from thorite in its rims and fracture zones.

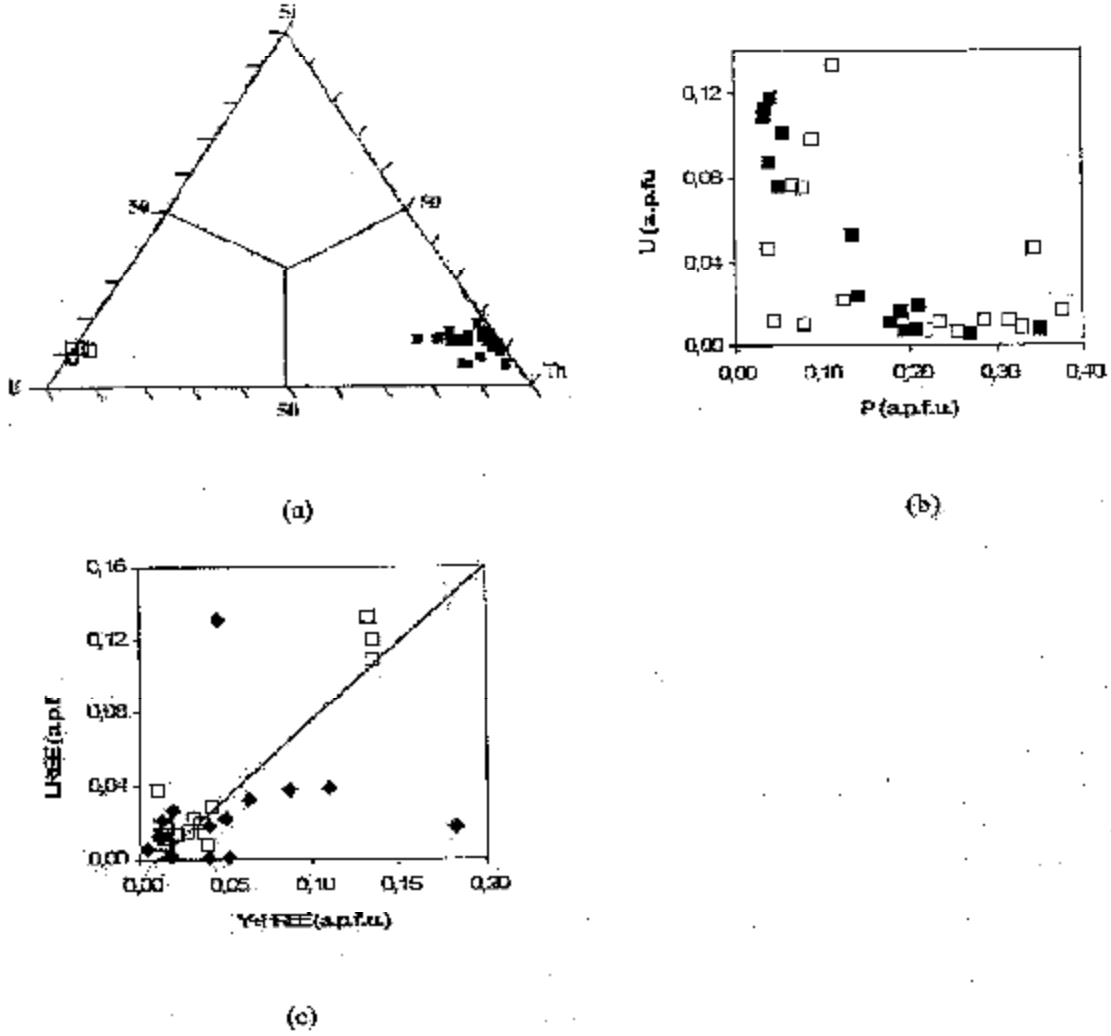

Figure 4. (a) – Composition of thorite and coffinite plotted on the basis of atom percentages in the U-Th-Si system. Symbols: open-coffinite, close- thorite. (b) – U versus P for thorite. Symbols: open-thorite from the unaltered granite, close- thorite from the altered granite. (c) – LREE versus Y+HREE. Symbols: open- thorite from the unaltered granite, close- thorite from the altered granite.

Ce-monazite is a primary mineral (Figure 2f) or it can be formed by metasomatic alteration of apatite (Figure 2t, u), which is also documented in the literature (HARLOV et al. 2002, 2005, HARLOV AND FORSTER 2003). Otherway it is replaced by thorite (Figure 2q, t, u, w). Replacement of monazite by thorite is reported by FINGER et al. (1998), TOWNSEND et al. (2000) and HETHERINGTON AND HARLOV (2008) found high huttonite ($ThSiO_4$) component in altered monazite. The textural evidence found in the altered granite indicates that some monazite was formed by apatite alteration and in turn some thorite was formed from monazite and apatite alteration.

Ce-monazite from the altered granite is poorer in U, Ca, Th , F and richer in Si and Al than Ce-monazite from the unaltered granite (Table 4), so the hydrothermal alteration of the granite caused removal of U, Th, F and Ca from the monazite. Altered monazite has a pervasive porosity (Figure 2f, q, w) and is replaced by thorite, but uraninite was not found in

this altered monazite, as reported by HETHERINGTON AND HARLOV (2008), due to the oxidizing conditions of the hydrothermal fluid. So some Th was incorporated in thorite, which precipitates in the fractures and pores of monazite but U was removed from monazite by the hydrothermal fluid, which agrees with HECHT AND CUNEY (2000). Monazite from hydrothermal quartz veins is texturally and chemically different from Ce-monazite of the unaltered granite. It has systematically lower Ca, U, Th, Y and higher Si; P, LREE than monazite from the unaltered granite (Table 4), because it is dissolved and has a hydrothermal origin. The analytical totals of monazite decrease from the unaltered granite to the altered granite and to mineralized quartz veins (Table 4), but the loss in U, Th and Y contents in the same direction are progressively much higher.

Xenotime from the unaltered granite is characterized by higher U contents than xenotime from the altered granite, and both have higher U contents than xenotime from hydrothermal veins (Table 3). In the altered granite, xenotime crystals are zoned, with cores richer in U than the respective rims (Table 3, Figure 3d) indicating loss of U in the crystal rims. So the hydrothermal alteration of granite caused a loss of U in xenotime, which was higher in the crystal rims.

Because of their similar ionic radii, rare earth elements (REE), particularly the heavy rare earth elements (HREE) substitute for Y in xenotime structure (WARK AND MILLER 1993, NI AND HUGHES 1995). The xenotime from the mineralized quartz veins is richer in Y and HREE than xenotime from the unaltered and altered granites (Table 3). In all xenotime crystals, the LREE contents are very low because they are not readily incorporated into the xenotime structure. Besides HREE, xenotime may accommodate significant concentrations of Th and U (HETHERINGTON et al. 2008). Uranium is always enriched relative to Th in the analysed xenotime and the highest Th content (mean of 0.014 apfu) was found in xenotime from the mineralized quartz veins, which has the lowest U contents (Table 3). There is so significant difference between the Th, Y and HREE contents of xenotime from the unaltered and altered granites, so the difference found in the U contents is due to alteration, indicating mobilization of U from xenotime structure, which is also supported by the fact that the rims of crystals are impoverished in U relatively to their cores (Table 3).

According to FÖRSTER (2006), the dominant complex coupled substitution in xenotime, involving both crystallographic sites in the lattice, is the thorite ($ThSiO_4$). Figures 2q and 2r show the intergrowth between xenotime and thorite. Compositional exchange between the two end-members, thorite and xenotime, is continuous because the minerals are iso-structural (HETHERINGTON et al. 2008), but the analysed xenotime has very low contents of Th (Table 3).

Although xenotime and monazite have different structures, they have some compositional and structural similarities (BROSKA et al. 2005). Figures 2q and r also show the intergrowth between xenotime and monazite, which have equal numbers of structural PO_4 tetrahedra and REO_8 polyhedra; however, monazite incorporates larger, light rare earth elements (LREE) in the REO_9 polyhedron (BROSKA et al. 2005).

In the altered granite and in the mineralized quartz veins, altered zircon is enriched in uranium. According to FÖRSTER (1999), uraninite is occasionally associated with zircon as minute inclusions or also as thin exsolutions, whose grain size does not allow accurate analysis. Uraninite included in zircon will promote its faster metamitization and alteration. Metamict zircon under hydrothermal conditions looses Si, U, Th and Pb (GEISLER et al. 2002, 2003). There is a significant loss of Si but a strong enrichment in U in the altered zircon

(Table 4). BSE image did not show concentrations of U in restricted areas within zircon grains but a continuous increase of U contents toward the altered rims and fractures of zircon crystals (Figure 2k in CABRAL PINTO et al. 2008). The oxidizing conditions of the hydrothermal fluid did not allow the precipitation of uraninite.

Zircon from the altered granite is richer in P, Fe, Y, U, La+Ce, Pb and poorer in Si, Zr, Hf, and has lower analytical totals than zircon from the unaltered granite. So the alteration of zircon is expressed by a decrease in Si, Zr, Hf, analytical totals and an increase in Fe, Y, La+Ce, Pb, U and P. In the altered granite, the core of zircon crystals have a chemical composition similar to zircon from the unaltered granite with very low or no uranium contents, but the crystal rims have up to 0.62 wt.% UO_2 and crystal rim from the mineralized quartz veins have up to 15.07 wt.% UO_2 (Table 3) but reaches 18 wt.% UO_2 (CABRAL PINTO et al. 2008). HORIE et al. (2008) also found gain in U in rims of altered zircon grains. The altered zircon and zircon rims also have high contents of P_2O_5 (Table 4). The enrichment in P is accompanied by enrichment in Y (Table 3) and HREE, promoting the formation of solid solutions with xenotime (DEER et al. 1997). The structural relationship between xenotime and zircon is reflected by their occurrence as intimate intergrowths in the related quartz veins (CABRAL PINTO et al. 2008). However, it should be noted that a few crystals show an impoverishment in U in their rims as found by GEISLER et al. (2002, 2003) in rims of altered zircon grains. The U-enrichment in rims of altered zircon grains in quartz veins is associated to the presence of Fe oxyhydroxides, which promoted the formation of new small U-phosphates at the margins of the altered zircon from U-rich supergenic solutions. Zircon in the altered granite, specially in the crystal rims is also rich in Fe (up to 0.66 wt.% Fe_2O_3, Table 3). So the enrichment in U is a compositional feature characteristic of altered zircon and is associated with high Fe contents (CABRAL PINTO et al. 2008).

Apatite from the altered granite and mineralized quartz veins is fractured and shows dissolution (Fig 2c,s-w,ac and Figure 3e) and is replaced by thorite, xenotime, and monazite, which fill fractures (Figure 2v, x, ac). Apatite from the altered granite is poorer in P, Ca, U, F and richer in Si, Th, Y, La and Ce than apatite from the unaltered granite (Table 4). So the hydrothermal alteration of apatite leads to a loss of P, Ca, U, F to the hydrothermal fluid, while the enrichment in Si, Th, Y, La and Ce leads to the formation of hydrothermal thorite, xenotime and monazite from apatite. Furthermore, the most fractured and altered crystals have very low analytical totals and show a significant loss in P (Table 4). In general, apatite from mineralized quartz veins is the richest in U and F (means of 0.13 wt.% UO_2 and 2.76 wt.% F, Table 4). Some apatite crystals associated with or replaced by uranium phosphates have the highest uranium contents (1.09 wt.% UO_2, Table 4), are richer in Fe, but its P contents are lower than those from apatite not associated with the U-phosphates.

Figure 2ad and Figure 3e show (meta)saleeite crystals growing at the surface of apatite, indicating the precipitation of (meta)saleeite at the reaction interfaces of dissolving apatite under local saturation. According to MURAKAMI et al. (1997), the observation that saleeite occurs where apatite have been replaced indicates that the local geochemical conditions in contact with apatite crystals are sufficient to precipitate saleeite at the expense of P by local saturation. Apatite is rare in quartz veins, probably due to its completely replacement by saleeite. The formation of the saleeite and meta-saleeite in the mineralized quartz veins is directly related to weathered apatite and Fe oxyhydroxides. The uranium was released during uraninite, coffinite, thorite, monazite, xenotime dissolutions and the phosphorus was released

essentially from apatite dissolution. The magnesium was released from chlorite alteration to clay minerals and Fe oxyhydroxides.

Chlorite from the altered granite is characterized by the average chemical formula $(Mg_{2.99}Fe_{5.87}Mn_{0.07}Al_{2.81})_{\Sigma 12.44}[(Si_{5.50}Al_{2.50})_{\Sigma 8.00}O_{20}](OH)_{16}$ (n=19), and is classified as clinochlore (BAILEY 1980). Uranium was not detected in this chlorite from altered granite, which has a Mg/(Mg+Fe) ratio of 0.34 (CABRAL PINTO, 2001). In the hydrothermal quartz veins, chlorite is clinochlore (BAILEY 1980). Chlorite occurs dispersed between quartz crystals has the average formula $(Mg_{4.76}Fe_{4.20}Mn_{0.05}Al_{2.82})_{\Sigma 11.83}[(Si_{5.34}Al_{2.66})_{\Sigma 8.00}O_{20}](OH)_{16}$ (n=26), a Mg/(Mg+Fe) ratio of 0.53 and contains 0.04 wt.% UO_2, but the clinochloe in contact with U-phosphates from these veins, has a composition $(Mg_{6.93}Fe_{2.42}Mn_{0.01}Al_{2.46}U_{0.01})_{\Sigma 11.83}[(Si_{5.62}Al_{2.38})_{\Sigma 8.00}O_{20}](OH)_{16}$ (n=6), a Mg/(Mg+Fe) ratio of 0.74, and on average 0.12 wt.% UO_2 (CABRAL PINTO et al. 2008).

The rims of chlorite crystals are richer in U than the respective cores and they are related with Fe oxyhydroxides with high contents of UO_2 (up to 5.63 wt.%), P_2O_5 (up to 7.07 wt.%), MgO (up to 2.5 wt.%) (CABRAL PINTO et al. 2008). The anatase was not found in the unaltered and altered granites, but it occurs in the hydrothermal quartz veins and is rich in U and its vacuoles and rims are replaced by U-bearing Fe oxyhydroxides (CABRAL PINTO et al. 2008). So the altered rims of chlorite and anatase from mineralized quartz veins are replaced by U-bearing Fe oxyhydroxides, containing up to 5.6 wt.% UO_2 and 3.7 wt.% P_2O_5), which may be due to nano-inclusions of U-phosphates (CABRAL PINTO et al. 2008).

CONCLUSIONS

The unaltered peraluminous Variscan granite contains uraninite and thorite. Uraninite is rare in the altered granite and some coffinite crystals show U impoverishment in their rims; so coffinite resulted from an early hydrothermal alteration of uraninite. Uranium-bearing minerals in the unaltered granite are thorite, xenotime, Ce-monazite; zircon and apatite also present some U. The textural, mineralogical and chemical changes found in this work show that uraninite, coffinite, thorite, xenotime, Ce-monazite, zircon, apatite, chlorite, anatase, from altered granite and/or hydrothermal mineralized quartz veins, are altered, dissolved, vacuolated and the rims of uraninite, coffinite, thorite, xenotime, Ce-monazite, are poorer in U than respective cores, indicating uranium removal to the fluid, while the altered rims of zircon, apatite, chlorite and anatase crystals are richer in U than respective cores. The enrichment in U is related to the presence of Fe minerals, Fe oxyhydroxides and altered apatite.

The U-mineralization in the quartz veins occurs in the intersection of two fault systems and the paragenetic sequence has three phases. The first phase originated silicates, sulphides and phosphates (apatite, xenotime, monazite), while the precipitation of the U-phosphates occurs in the third supergenic phase (CABRAL PINTO et al. 2008). The large and deep Variscan faults were reactivated by the Alpine tectonism and gave rise to a deep circulation of meteoric waters within the granite, and along the quartz veins, which were heated up and became enriched in uranium by solubilisation, and locally the completely remobilization of U-bearing minerals (COTELO NEIVA 2003). These hot meteoric fluids dissolved (the remaining) uraninite, coffinite, thorite, monazite, and xenotime, apatite in the biotite granite

and apatite, monazite, xenotime in the quartz veins and became enriched in U and P. These fluids were responsible for the growth of a new mineral assemblage in the hydrothermal quartz veins, where the dissolved U was fixed on the altered surface of minerals, like zircon and apatite, by adsorption (HECHT AND CUNEY 2000), or by precipitation as uranium minerals, such as saleeite and meta-saleeite. According to DE PUTTER et al. (1998), the neoformation of discrete minerals on high-surface area weathering products, rather than direct elemental adsorption, could be a major mechanism in U secondary concentration.

Phosphorous resulted from the dissolution of apatite, monazite and xenotime from the granite and mineralized quartz veins and Mg was released to the fluid mostly by chlorite alteration. The precipitation of U-phosphates occurred at the surface of anatase and Fe oxyhydroxides, released from altered chlorite and sulphides, and at the altered apatite surface. MURAKAMI et al. (1997) also reported the precipitation of microcrystals of (meta)saleeite at the surface of Fe minerals even where groundwater U concentrations are low, as in the study area. As groundwater is undersaturated with respect to uranyl phosphates, such as saleeite (PINTO et al. 2004), simple solubility-controlled precipitation was not the major mechanism, but only one for the formation of the mineralization (CABRAL PINTO et al. 2008). This precipitation at the surface of the new Fe-minerals was the main factor responsible for U retention within the quartz veins leading to the uranium phosphate mineralization of Vale de Abrutiga (CABRAL PINTO AND SILVA 2007). However, saleeite was also found replacing U-rich apatite (Fig 2ad) and apatite is rare in the mineralized quartz veins, because it was replaced by monazite and by U-phospahtes. The hydrothermal fluid is rich in U and Mg and saleeite and meta-saleeite precipitated at apatite weathered surface. The immobilization of U(VI) from aqueous solutions in a solid phase by interaction with apatite has been studied (ORDOÑEZ-REGIS et al. 1999, AREY et al. 1999, THOMSON et al. 2003, JEANJEAN et al. 2005, CONCA AND WRIGHT 2006, SIMON et al. 2008, WELLMAN et al. 2008), and the dominant mechanisms are: dissolution-precipitation or sorption onto the apatite surface with formation of amorphous or microcrystalline U phases (JEANJEAN et al. 2005, SIMON et al. 2008).

The uranium released from uraninite (and thorite?) in the early hydrothermal alteration of the granite was immobilized in coffinite. Later, meteoric hot fluids, circulating through reactivated deep faults, promoted a high dissolution of (remaining) uraninite, coffinite, thorite, xenotime, monazite in the granite and became enriched in uranium. The alteration of monazite and apatite from the granite and the mineralized quartz veins released P to the fluid, while Mg and Fe were released from the weathering of chlorite and sulphides.

Close to the surface, where oxygen content is high, the brecciated quartz veins are structural traps where Fe is immobilized as Fe oxyhydroxides. These Fe oxyhydroxides precipitated in fractures, pores and rims of the altered zircon, anatase and chlorite. The precipitation of U-phosphates occurs at the surface of these Fe oxyhydroxides and in the weathered surface of apatite, immobilizing the uranium. The Fe- oxyhydroxides can also have adsorbed some U, P and Mg, and its transformation to hematite or goethite leads to the precipitation of U-phosphate minerals. The uptake of U by Si/Al/Fe gels could also occur (CABRAL PINTO et al. 2008).

ACKNOWLEDGEMENTS

Thanks are due to Prof B.J. WOOD for the EUGF – Bristol Facility contract ERBFMGECT 980128 for the use of the electron-microprobe at the University of Bristol, U. K.; Prof. M.R. MACHADO LEITE and Dr. J.M. FARINHA RAMOS for the use the electron-microprobe at the Geological and Mining Institute, S. Mamede de Infesta, Portugal; ENU Administration for having provided the rock samples; Prof JORGE BRITO for all the support given throughout this work. This research was carried out in the programme of GEOSCIENCES CENTRE, UNIVERSITY OF COIMBRA, PORTUGAL, and of UNIVERSITY JEAN PIAGET OF CAPE VERDE (PIAGET INSTITUTE).

REFERENCES

Abdelouas, A., Lutze, W., Nuttall, H.E. (1999): Uranium contamination in the subsurface; characterization and remediation. *Reviews in Mineralogy and Geochemistry* – 38(1): 433-473.

Arey , J.S., Seaman, J., Bertch, P.M. (1999): Immobilization of Uranium in Contaminated Sediments by Hydroxyapatite Addition. – *Environ. Sci. Technol.* 33: 337-342.

Bailey, S. W. (1980): Summary of recommendations of AIPEA nomenclature committee. – *Clay Minerals* 15: 85-93.

Basham, I.R., Ball, T.K., Beddoe-Stephens, B.,d Michie, U.McL. (1982): Uranium-bearing accessory minerals and granite fertility: II. Studies of granites from the British Isles. In: Compte-rendu methodes de prospection de l'uranium; Symposium sur les methodes de prospection de l'uranium — examen dur programme AEN - AIEA de R and D. *Organ. Econ. Coop. and Develop.*, Paris, 398-413.

Broska, I., Williams, C.T., Geza Nagy, M.J. (2005): Alteration and breakdown of xenotime-(Y) and monazite-(Ce) in granitic rocks of the Western Carpathians, Slovakia. – Lithos 82: 71–83.

Bruno, J. and Ewing, R.C. (2006): Spent nuclear fuel. – Elements 2: 343–349.

Burns, P.C. and Finch, R. (1999): Uranium: Mineralogy, Geochemistry and the environment. – *Reviews in Mineralogy* 38: 679 pp.

Cabral Pinto, M.M.S. and Silva, M.M.V.G. (2007): The Vale de Abrutiga uranium phosphates mine, central Portugal. – Chem. Erde. 67 (3): 251–252.

Cabral Pinto, M.M.S. (2001): Mineralizações uraníferas do Vale de Abrutiga e impacte ambiental da sua exploração. – MsC thesis. University of Coimbra. 312 pp.

Cabral Pinto, M.M.S., Silva, M.M.V.G., Neiva, A.M.R. (2008): Geochemistry of U-bearing minerals from the Vale de Abrutiga uranium mine area, Central Portugal. – N. Jb. Mineralogie. 185(2): 183-198.

Conca, J.L. and Wright, J. (2006): An apatite II permeable reactive barrier to remediate groundwater containing Zn, Pb and Cd. – *Appl. Geochem.* 21: 1288–1300.

Cotelo Neiva, J.M. (2003): Jazigos portugueses de minérios de urânio e sua génese. – In Engineering Geology and Geological Resources, Book in honour to Prof. J. M. Cotelo Neiva. M.R.P.V. Ferreira (Editor). Coimbra University Press (written in Portuguese) 1: 15–76.

Cuney, M. and Friederich, M. (1987): Physicochemical and crystal-chemical controls on accessory mineral paragenesis in granitoids: implications for uranium metallogenesis. – *Bull. Minerl.* 110: 235–247.

Deer, W.A., Howie, R.A., Zussman, J. (1997): Rock-forming minerals – Orthosilicaes, Vol 1A (2nd edition). London: The Geological Society 919 pp.

De Putter, T., Charlet, J.M., Quinif, Y. (1999): REE, Y and U concentration at the fluid-iron oxide interface in late Cenozoic cryptodolines from Southern Belgium. *Chemical Geology* 153: 139–150.

Deditius, A.P., Utsunomiya, A., Ewing, R.C. (2007): Fate of trace elements during alteration of uraninite in a hydrothermal vein-type U-deposit from Marshall Pass, Colorado, USA. – *Geochimica et Cosmochimica Acta 71*: 4954–4973.

Evins, L.Z., Jensen, A.K., Ewing, R.C. (2005): Uraninite recrystallization and Pb loss in the Oklo and Bangombe natural fission reactors, Gabon. – *Geochimica et Cosmochimica* Acta 69(6):1589-1606.

Fayek, M., Janeczek, J., Ewing, R.C. (1997): Mineral chemistry and oxygen isotopic analyses of uraninite, pitchblende and uranium alteration minerals from the Cigar lake deposit, Saskatchewan, Canada. – *App. Geochem.* 12: 549–565.

Finch, R. and Murakami, T. (1999): Systematics, Paragenesis of U minerals. In Uranium: Mineralogy, Geochemistry and the Environment. – *Reviews in mineralogy* 38: 91–180. Burns P. C., Finch R. (Eds). Ribbe P. H. (Series Editor).

Finch, R.J. and Ewing, R.C. (1992): The corrosion of uraninite under oxidizing conditions. – *J. Nucl. Mater.* 190: 133–156.

Finger, F., Broska, I., Roberts, M.P., Schermaier, A. (1998): Replacement of primary monazite by apatite-allanite-epidote coronas in an amphibolite facies granite gneiss from the eastern Alps. – American Mineralogist 83: 248–258.

Fleischer, M. and Mandarino, J.A. (1995): Glossary of Mineral Species 1995. The Mineralogical Record, Tucson, Arizona.

Förster, H.-J. (1999): The chemical composition of uraninite in Variscan granites of the Erzgebirge, Germany. – *Mineral Mag.* 63: 239- 52.

Förster, H.-J. (2006): Composition and origin of intermediate solid solutions in the system thorite–xenotime–zircon–coffinite. – *Lithos* 88: 35–55.

Förster, H.-J. (1999): The chemical composition of uraninite in Variscan granites of Erzgebirge, Germany. – *Mineral. Mag.* 63: 239–252.

Gaines, R.V., Skinner, H.C.W., Foord, E.E., Mason, B., Rosenzweig, A., King, V.T., Dowty, E. (1997): Dana's New Mineralogy, 8th Edition. Wiley and Sons, New York, 1819 pp.

Geisler, T., Pidgeon, R.T., Kurtz, R., van Bronswijk, W., Schleicher, H. (2003): Experimental hydrothermal alteration of partially metamict zircon. – *Amer. Mineral.* 88: 1496–1513.

Geisler, T., Pidgeon, R.T., van Bronswijk, W., Kurtz, R. (2002): Transport of uranium, thorium, and lead in metamict zircon under low-temperature hydrothermal conditions. – *Chem. Geol.* 191: 141–154.

Grandstaff, D.E. (1976): A kinetic of the dissolution of uraninite. – *Econ. Geol.* 71: 1493–1506.

Harlov, D.E., Andersson, U.B., Förster, H-J, Nyström, J.O., Dulski, P., Broman, C. (2002): Apatite–monazite relations in the Kiirunavaara magnetite–apatite ore, northern Sweden – *Chemical Geology* 191:47-72.

Harlov, D.E.,Wirth, R., Förster, H.-J. (2005): An experimental study of dissolution–reprecipitation in fluorapatite: fluid infiltration and the formation of monazite. – *Contrib. Mineral. Petrol.* 150: 268–286.

Harlov, D.E. and Förster, H-J. (2003): The role of accessory minerals in rocks: Petrogenetic indicators of metamorphic and igneous processes. – Lithos 95: 7-10

Hecht, L. and Cuney, M. (2000): Hydrothermal alteration of monazite in the Precambrian crystalline basement of the Athabasca Basin (Saskatchewan, Canada): implications for the formation of unconformity-related uranium deposits. – *Mineral. Deposita* 35: 791–795.

Hetherington, C.J. and Harlov, D.E. (2008): Metasomatic thorite and uraninite inclusions in xenotime and monazite from granitic pegmatites, Hidra anorthosite massif, southwestern Norway: Mechanics and fluid chemistry. – American Mineralogist 93: 806–820.

Hetherington, C.J., Jercinovic, M.J., Williams M.L., Mahan. K., (2008): Understanding geologic processes with xenotime: composition, chronology, and protocol for electron probe microanalysis. DOI:10.1016/j.chemgeo.2008.05.020, Reference: CHEMGE 15402.

Hsi, C-K.D. and Langmuir, D. (1985): Adsorption of uranyl onto ferric oxyhydroxides: Aplication of the surface complexation site-binding model. – Geochimica et *Cosmochimica Acta.* 49: 1931-1941.

Horie, K, Hidakab, H., Gauthier-Lafaye, F. (2008): Elemental distribution in apatite, titanite and zircon during hydrothermal alteration: Durability of immobilization mineral phases for actinides. – *Physics and Chemistry of the Earth* 33 962–968.

Janeczek, J. and Ewing, R.C. (1991): X-ray powder diffraction study of annealed uraninite. – *Journal of Nuclear Materials* 185 (1): 66-77.

Janeczek, J. and Ewing, R.C. (1992A): Structural formula of uraninite. – *J. Nucl. Mater.* 190: 128–132.

Janeczek, J. and Ewing, R.C. (1992b): Dissolution and alteration of uraninite under reducing conditions. – *J. Nucl. Mater.* 190: 157–173.

Jeanjean, J., Rouchaud, J.C., Tran, L., Fedoroff, M. (2005): Sorption of uranium and other heavy metals on hydroxyapatite – *Journal of Radioanalytical and Nuclear Chemistry* 201: 529-539.

Jensen, K.A. and Ewing, R.C. (2001): The Okelobongo natural fission reactor, southeast Gabon: Geology, mineralogy, and retardation of nuclear-reaction products. – *GSA Bull.* 113. 32–62.

Jensen, K.A., Ewing, R.C., Gauthier-Lafaye, F. (1997): Uraninite: a 2 Ga spent nuclear fuel from the natural fission reactor at Bangombe Lir. Gabon, West Africa. – *Mat. Res. Soc. Symp. Proc.* 465: 1209–1218.

Jerden Jr, J. L. and Sinha, A. K. (2003): Phosphate based immobilization of uranium in an oxidizing bedrock aquifer. – *Appl. Geochem.* 18: 823–843.

Kotzer, T. G. and Kyser, T. K. (1993): O, U, and Pb isotopic and chemical variations in uraninite: Implications for determining the temporal and fluid history of ancient terranes. – *Am. Mineral.* 78: 1262–1274.

Langmuir, D. (1978): Uranium solution-mineral equilibria at low temperatures with applications to sedimentary ore deposits. – *Geochim. Cosmochim. Acta* 42: 547–569.

Lottermoser, B.G. and Ashley, T.P.M. (2005): Tailings dam seepage at the rehabilitated Mary Kathleen uranium mine, Australia. – *Journal of Geochemical Exploration* 85:19-137.

Lumpkin, G.R. and Chakoumakos, B.C. (1988): Chemistry and radiation effects of thorite-group minerals from the Harding pegmatite, Taos County, New Mexico. – American Mineralogist 73: 1405–1419.

Matos Dias, J.M. (1982): Perspectivas geoeconómicas dos jazigos uraníferos portugueses. – *Geonovas* 1(3): 33-39.

Murakami, T., Ohnuki, T., Isobe, H. (1997): Mobility of uranium during weathering. – *Am. Miner.* 82: 888–899.

Murphy, W. M. and Shock, E. L. (1999): Environmental Aqueous Geochemistry of Actinides. In Uranium: Mineralogy, Geochemistry and the Environment In Reviews in mineralogy, 38. Burns P. C., Finch R. (Eds). Ribbe P. H. (Series Editor). P.221 -253.

Ni, Y. and Hughes, J.M. (1995): Crystal chemistry of the monazite and xenotime structures. – American Mineralogist 80: 21-26.

Ordoñez-Regis, E., Romero Guzmán, E.T., Ordoñez Regil En (1999): Surface modification in natural fluorapatite after uranyl solution treatment. – *Journal of Radioanalytical and Nuclear Chemistry* 240 (2): 541-554.

Pagel, M. (1981): Acteurs de distribuition et concentration de l'uranium et du thorium dans quelques granites de la chaine Hercynienne d'Europe. PhD thesis. L'Institut National Polytechnique de Lorraine. 566 pp.

Parks, G.A. and Pohl, D.C. (1988): Hydrothermal solubility of uraninite. – *Geochim. Cosmochim. Acta* 52: 863–875.

Pearcy, E.C., Prikryl, J.D., Murphy, W.M., Leslie, B.W. (1994): Alteration of uraninite from the Nopal I deposit, Peña Blanca District, Chihuahua, Mexico, compared to degradation of spent nuclear fuel in the proposed U.S. high-level nuclear waste repository at Yucca Mountain, Nevada. – *App. Geochem.* 9: 713–732.

Pinto, M. M. S. C., Silva, M. M. V. G., Neiva, A. M. R. (2004): Pollution of Water and Stream Sediments associated with the Vale de Abrutiga Uranium mine, Central Portugal. – *Journal Mine Water and the Environment* 23: 66–75.

Plant, J.A., Simpson, P.R., Smith, B. and Windley, B.F. (1999): Uranium ore deposits-products of the radioactive earth. Uranium: Mineralogy, Geochemistry and the Environment. In Uranium: Mineralogy, Geochemistry and the Environment, vol. 38 (eds. P. C. Burns and R. J. Finch). *Rev. Mineral.*, pp. 255–319.

Poty, B., Leroy, J., Cathelineau, M., Cuney, M., Friedrich, M., Lespinasse, M., Turpin, L. (1986): Uranium deposits spatially related to granites in the French part of the Hercynian orogen. In Vein Type Uranium Deposits, IAEA-TC-361, *International Atomic Energy Agency*, Vienna, 215-246.

Rubin, J.N., Henry, C.H., Price, J.G. (1989): Hydrothermal zircons and zircon overgrowths, Sierra Blanca Peaks, Texas. –American Mineralogist 74: 865–869.

Silva, M.M.V.G. and Neiva A.M.R., (1999/2000): Geochemistry of Hercynian peraluminous granites and their minerals from Carregal do Sal-Nelas-Lagares da Beira area, Central Portugal. – *Chem. Erde* 59: 329 -349.

Silva, M.M.V.G., Neiva, A.M.R., Whitehouse, M.J. (2000): Geochemistry of enclaves and host granites from the Nelas area, central Portugal. – Lithos 50: 153 -170.

Simon, F.G., Biermann, V., Peplinski, B. (2008): Uranium removal from groundwater using hydroxyapatite. *Applied Geochemistry* 23: 2137–2145.

Smith Jr, D.K. (1984): Uranium mineralogy. In Uranium Geochemistry, Mineralogy, Geology, Exploration and Resources. De Vivo B., Ippolito F., Capaldi G., Simpson P.R. (Eds). Institute of Mining and Metallurgy, London, 43–88.

Smits, G. (1989): (U,Th)-bearing silicates in reefs of the Witwatersrand, South Africa. – Canadian Mineralogist 27: 643 – 655.

Speer, J.A., (1982): The actinide orthosilicates. In: Ribbe, P.H. (Ed.). Orthosilicates. – Reviews in Mineralogy 5: 113– 135. Mineralogical Society of America, Washington, DC.

Tischendorf, G. and Förster, H.-J. (1994): Hercynian granite magmatism and related metallogenesis in the Erzgebirge: A status report. In Mineral Deposits of the Erzgebirge/Krusnehory(Germany/Czech Republic) (Kv. Gehlen and D.D. Klemm, eds.). – *Monograph Series on Mineral Deposits* 31: 5-23.

Thomson, B.M., Smith, C.L., Busch, R.D., Siegel, M.D. (2003): Removal of Metals and Radionuclides Using Apatite and Other Natural Sorbents – *J. Envir. Engrg.* 129(6): 492 - 499

Townsend, K.J., Miller, C.F., D'Andrea, J.L., Ayers, J.C., Harrison, T.M., Coath, C.D. (2000): Low temperature replacement of monazite in the Ireteba granite, Southern Nevada: geochronological implications. – *Chem. Geol.* 172: 95– 112.

Wark, D.A., Miller, C.F. (1993): Accessory mineral behavior during differentiation of a granite suite: monazite, xenotime and zircon in the Sweetwater Wash pluton, southeastern California, U.S.A. – *Chemical Geology* 110: 49-67.

Wellman D.M., Gloveck, J.N., Parker, K., Richards, E.L., Pierce, E.M. (2008): Sequestration and retention of uranium(VI) in the presence of hydroxylapatite under dynamic geochemical conditions. – *Environmental Chemistry* 5(1): 40–50.